POLITECNICO DI TORINO
Repository ISTITUZIONALE

The scattering of electromagnetic waves by two opposite staggered perfectly electrically conducting half-planes

*Original*
The scattering of electromagnetic waves by two opposite staggered perfectly electrically conducting half-planes / Daniele, V. G.; Lombardi, G.; Zich, R. S.. - In: WAVE MOTION. - ISSN 0165-2125. - STAMPA. - 83:(2018), pp. 241-263. [10.1016/j.wavemoti.2018.09.017]

*Availability:*
This version is available at: 11583/2721544 since: 2018-12-21T16:49:13Z

*Publisher:*
Elsevier B.V.

*Published*
DOI:10.1016/j.wavemoti.2018.09.017

*Terms of use:*

This article is made available under terms and conditions as specified in the corresponding bibliographic description in the repository

*Publisher copyright*
Elsevier postprint/Author's Accepted Manuscript

© 2018. This manuscript version is made available under the CC-BY-NC-ND 4.0 license
http://creativecommons.org/licenses/by-nc-nd/4.0/.The final authenticated version is available online at:
http://dx.doi.org/10.1016/j.wavemoti.2018.09.017

(Article begins on next page)

19 April 2024

# The scattering of electromagnetic waves by two opposite staggered perfectly electrically conducting half-planes

V.G. Daniele, G. Lombardi*, R.S. Zich

*Politecnico di Torino-ISMB, Torino, Italy*

**Abstract**

In this paper we examine the scattering of a plane electromagnetic wave by two opposite staggered perfectly electrically conducting (PEC) half-planes immersed in free space by using the Wiener-Hopf technique in the spectral domain. The procedure to obtain the solution is based on the reduction of the factorization problem of matrix Wiener-Hopf equations to Fredholm integral equations of second kind (Fredholm factorization). The structure is of interest in antenna technologies, electromagnetic compatibility and electromagnetic shielding in particular for the computation of the transmitted field.

*Keywords:* Electromagnetic scattering, Diffraction, Wiener-Hopf method, Integral equations, Network modelling, Stratified regions, Half-planes, Analytical-numerical methods, Antenna technologies, Electromagnetic compatibility, Electromagnetic shielding

## 1. Introduction

In this paper we consider the classical canonical scattering problem constituted of two opposed staggered Perfectly Electrically Conducting (PEC) half planes immersed in free-space. Cartesian coordinates as well as polar coordinates will be used to describe the problem. Two origins are considered, see Fig. 1: the edge of the upper half-plane is chosen as origin $O$ for coordinates

*Corresponding author
*Email address:* guido.lombardi@polito.it (V.G. Daniele, G. Lombardi*, R.S. Zich)

$(x, y, z)$ and $(\rho, \varphi, z)$, while the edge of the lower half-plane is chosen as origin $O'$ for coordinates $(x_2, y_2, z_2)$ and $(\rho_2, \varphi_2, z)$. The two reference systems are related through the following relations: $x_2 = x - s,\ y_2 = y + d$. Fig.1 shows the two PEC half planes with zero thickness respectively defined by $x < 0, y = 0, -\infty < z < +\infty$ and $x > s, y = -d, -\infty < z < +\infty$; thus the problem is with translational symmetry along the z axis. In the following we will consider $s$ as the staggered parameter along $x$ and $d$ as the distance along $y$ between the two half-planes. While $d$ can assume only positive values, $s$ can be either positive as in Fig. 1 or negative. In the last case, the two half-planes partially overlap and generate a section of parallel PEC plane waveguide of length $|s|$. Three regions are identified: region 1 is the half space region delimited by $y > 0$, region 2 is the rectangular finite region with $-d < y < 0$ and region 3 is the half space region delimited by $y < -d$. For the sake of simplicity, the structure is illuminated by an $E_z$-polarized plane wave from region 1 with azimuthal direction $\varphi = \varphi_o$ and with propagation constant $k$:

$$E_z^i = E_o e^{jk\,\rho\cos(\varphi - \varphi_o)} \tag{1}$$

The literature shows several works that are related to this problem. In particular we took inspiration by the works of Abrahams on water waves [1]-[3] that study the problem via matrix Wiener-Hopf equations. These formulations highlight the presence of problematic exponential behavior of the spectral unknowns depending on the staggered parameter $s$. Another attempt to deal with exponential factors is reported in [4]. Classical related problems are the diffraction by three semi-infinite planes by Jones [5] or the problems described in [6]-[11]. The matrix Wiener-Hopf equations of staggered problems show the presence of exponential phase factors that needs special attention to obtain an effective solutions. Solutions are proposed in [12]-[14] and [1]-[4] where specialized techniques are proposed according to the sign of the staggered parameters $s$ (i.e. $s < 0$ overlapping half-planes, $s > 0$ non overlapping half planes). In fact discrete spectrum (poles) together with continuous spectrum is present for $s < 0$ since a parallel PEC plane waveguide of length $|s|$ is generated. On the

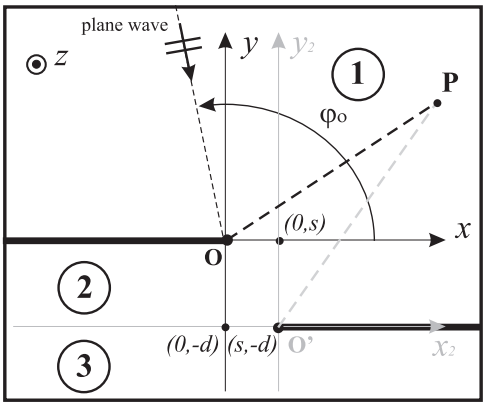


Figure 1: Scattering of an electromagnetic wave by two opposite staggered PEC half-planes. Two cartesian reference systems are reported in the figure with coordinates $(x, y, z)$ and $(x_2, y_2, z)$ and centered respectively in $O$ and $O'$. They are related through the following relations: $x_2 = x - s$, $y_2 = y + d$. Cylindrical coordinates $(\rho, \varphi, z)$ centered in $O$ and $(\rho_2, \varphi_2, z)$ centered $O'$ are used too. The figure represent the non-overlapped case with positive $s$, although the proposed method is valid for any $s$ and positive $d$.

contrary for $s > 0$ only continuous spectrum is present.

With reference to the structure under investigation (Fig. 1), in this work we provide a general effective procedure for the solution of the problem for any $s$ and any positive $d$, i.e. the overlapped and non-overlapped cases. As in most of papers devoted to this problem, we start assuming the formulation in terms of matrix Wiener-Hopf equations in spectral domain for an arbitrary value of $s$ [1]-[4], [10], [12]. However, the procedure to obtain the solution of the WH equations is different from that of the other authors (weak factorization) because it is based on the reduction of the factorization problem to Fredholm integral equations of second kind. We call this factorization technique *Fredholm factorization*. This technique has been studied in [15]-[16] and effectively applied in several scattering problems [19]-[21],[25]-[28]. The spectral formulation of the problem reported in the following sections will take into consideration the interaction at near field of the edges of the two edges located at $(x, y) = (0, 0)$ and $(x, y) = (s, -d)$ by using a comprehensive mathematical model, i.e. a model that considers all the physical interactions of the problem together.

Focusing the attention on separated half-planes, the literature presents also alternative solutions based on multiple diffractions starting from the standard Geometrical Theory of Diffraction (GTD) scattering model of the single diffractive structure [29]-[31].

The solution steps of the method proposed in this paper are: 1) formulation via the Wiener-Hopf (WH) technique with the help of network modelling [16]-[20], 2) the Fredholm factorization [15]-[16] and 3) asymptotic estimations of electromagnetic field [22]. The complementary use of network modeling (although not essential) mathematically rephrases the spectral representations and it yields the advantage of a direct and quick pictorial interpretation of the interaction among structures that constitute the original problem. Moreover, in general, network modelling orders and systematizes the steps necessary to obtain the spectral equations of complex scattering problems avoiding redundancy in different applications [16]-[20].

The paper is divided into seven Sections including the introduction. Section 2 presents the mathematical definitions and background preparatory to the Wiener-Hopf equations of the three regions reported in Section 3. The same Section also shows the reduction of the equations to integral representations. Both Wiener-Hopf equations and the integral representations derived during the Fredholm factorization can be easily interpreted as network relations. In Section 4 the integral representations allow to obtain the factorization of the problem and the solution via Fredholm factorization in terms of spectra. In particular Fredholm integral equations of second kind are derived. Section 5 focuses the attention on how to estimate physical/engineering quantities. Finally Section 6 provides validation and convergence of the proposed method and it compares our results with the ones obtained by a full numerical technique demonstrating the superiority of the proposed semi-analytical technique for infinite canonical problems. The same section discusses the properties of the solution in practical cases and it presents physical and engineering insights for applications in the field of antenna technologies, electromagnetic compatibility and electromagnetic shielding: GTD/UTD diffraction coefficients (UTD=Uniform Theory of

Diffraction), total far fields, transmitted scattered energy flux. Conclusions are reported in Section 7.

## 2. Mathematical Definitions and Background

For the sake of simplicity, the structure is illuminated by an $E_z$-polarized plane wave from region 1. The general skew incidence case does not introduce conceptual difficulties but doubles the number of equations to be solved.

Taking into account the geometry and the sources, the total field is independent of $z$ and we have non null field components $E_z(x,y), H_x(x,y), H_y(x,y)$. In this case the wave equation governs the field components, in particular for the electric field we have

$$\partial^2 E_z/\partial x^2 + \partial^2 E_z/\partial y^2 + k^2 E_z = 0 \tag{2}$$

where $k$ is the free-space propagation constant. To meet mathematical requirements of the WH technique small vanishing losses are assumed in the medium, i.e. $k = k' - jk''$ where $k', k'' > 0$ and $k''/k' << 1$ (negligible losses).

The boundary conditions of the problem are: 1) zero $E_z$ on the perfect conductors, i.e. $E_z(x, y = 0_-) = 0$ for $x < 0$, $E_z(x, -d_+) = 0$ for $x > s$; and 2) continuity of both $E_z$ and $H_x$ on the interfaces $y = 0, x > 0$ and $y = -d, x < s$, i.e. $E_z(x, 0_-) = E_z(x, 0_+)$ for $x > 0$, $H_x(x, 0_-) = H_x(x, 0_+)$ for $x > 0$, $E_z(x, -d_-) = E_z(x, -d_+)$ for $x < s$, $H_x(x, -d_-) = H_x(x, -d_+)$ for $x < s$. To clarify the notation we consider $y = 0_\pm = \pm\delta$ and $y = -d_\pm = -d \pm \delta$ with positive vanishing $\delta$.

On the upper half plane as $\rho \to 0$, $E_z(\rho, \varphi)$ remains finite (Meixner's edge condition [23]): $E_z(\rho, \varphi) = M_0 + O(\rho^m)$ with constant $M_0$ and $m > 0$. We have same behavior for the lower half-plane.

In region 1 the following radiation condition holds: $\left|E_z(\rho, \varphi) - E_z^{GO}(\rho, \varphi)\right| \leq e^{-a_1 \rho}$ with $a_1 > 0$ and where $E_z^{GO}$ is the Geometrical Optics component of $E_z$. We have same behavior in region 3 without the presence of GO field.

According to the uniqueness theorem, the solution fulfills the edge and the radiation conditions.

The starting point to deduce the matrix Wiener-Hopf equations of the problem is to subdivide the entire geometry into three planar regions bounded by the two half plane interfaces, see Fig. 1. As reported in the figure, we consider two reference systems for cartesian coordinates (and polar coordinates) and we define the electromagnetic quantities using the following notation

$$\dot{\mathbf{E}}(x_2, y) = \mathbf{E}(x, y),\ \dot{\mathbf{H}}(x_2, y) = \mathbf{H}(x, y) \tag{3}$$

To derive the formulation of the problem in the spectral domain we define the following Laplace transforms at $y = 0_\pm, -d_\pm$:

$$\begin{cases} V_{1+}(\eta) = \int\limits_0^\infty E_z(x, 0_\pm) e^{j\eta\, x} dx \\ I_{1+}(\eta) = \int\limits_0^\infty H_x(x, 0_\pm) e^{j\eta\, x} dx \end{cases} \tag{4}$$

$$\begin{cases} V_{2\pi+}(\eta) = \int\limits_{-\infty}^0 \dot{E}_z(x_2, -d_\pm) e^{-j\eta\, x_2} dx_2 = e^{j\eta\, s} \int\limits_{-\infty}^s E_z(x, -d_\pm) e^{-j\eta\, x} dx \\ I_{2\pi+}(\eta) = -\int\limits_{-\infty}^0 \dot{H}_x(x_2, -d_\pm) e^{-j\eta\, x_2} dx_2 = -e^{j\eta\, s} \int\limits_{-\infty}^s H_x(x, -d_\pm) e^{-j\eta\, x} dx \end{cases} \tag{5}$$

$$\begin{cases} V_{1\pi+}(\eta) = \int\limits_{-\infty}^0 E_z(x, 0_-) e^{-j\eta\, x} dx = 0 \\ V_{a-}(\eta) = \int\limits_{-\infty}^0 E_z(x, 0_+) e^{j\eta\, x} dx = 0 \\ I_{1\pi+}(\eta) = -\int\limits_{-\infty}^0 H_x(x, 0_-) e^{-j\eta\, x} dx \\ I_{a-}(\eta) = \int\limits_{-\infty}^0 H_x(x, 0_+) e^{j\eta\, x} dx \end{cases} \tag{6}$$

$$\begin{cases} V_{2+}(\eta) = \int\limits_0^\infty \dot{E}_z(x_2, -d_+) e^{j\eta\, x_2} dx_2 = e^{-j\eta\, s} \int\limits_s^\infty E_z(x, -d_+) e^{j\eta\, x} dx = 0 \\ V_{d+}(\eta) = \int\limits_0^\infty \dot{E}_z(x_2, -d_-) e^{j\eta\, x_2} dx_2 = e^{-j\eta\, s} \int\limits_s^\infty E_z(x, -d_-) e^{j\eta\, x} dx = 0 \\ I_{2+}(\eta) = \int\limits_0^\infty \dot{H}_x(x_2, -d_+) e^{j\eta\, x_2} dx_2 = e^{-j\eta\, s} \int\limits_s^\infty H_x(x, -d_+) e^{j\eta\, x} dx \\ I_{d+}(\eta) = \int\limits_0^\infty \dot{H}_x(x_2, -d_-) e^{j\eta\, x_2} dx_2 = e^{-j\eta\, s} \int\limits_s^\infty H_x(x, -d_-) e^{j\eta\, x} dx \end{cases} \tag{7}$$

In order to quickly understand the support of the Laplace transforms Fig. 2 shows a pictorial representation of the Laplace transforms of $H_x$ (the currents). In particular we note that the support of $I_{a-}$, $I_{1\pi+}$, $I_{2+}$ and $I_{d+}$ is on one face

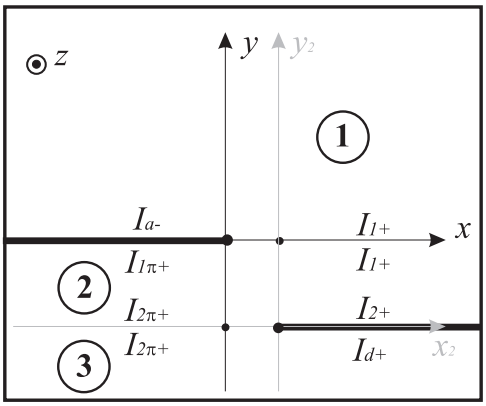


Figure 2: Pictorial interpretation of the support of Laplace transforms of $H_x$ as defined in (4)-(7).

of the half planes (either upper or lower face), on the contrary $I_{1+}$ and $I_{2\pi+}$ are defined on the interface between regions. The boundary conditions of the PEC half planes are enforced by nullifying the quantities related to the electric field on the PEC faces, i.e. $V_{1\pi+}, V_{a-}, V_{2+}, V_{d+}$ are zero.

These quantities are labeled with $\pm$ subscripts: $+$ indicates plus functions in the complex plane $\eta$, *i.e.* functions that converge in an upper half-plane ($Im[\eta] > Im[\eta_{up}]$); conversely $-$ indicates minus functions that converge in a lower half-plane ($Im[\eta] < Im[\eta_{lo}]$). The $+$ $(-)$ functions are considered non-conventional (non-standard) if $Im[\eta_{up}] > 0$ ($Im[\eta_{lo}] < 0$). The non-standard singularities are those located in $Im[\eta] > 0$ for plus functions and in $Im[\eta] < 0$ for minus functions. Assuming propagation constants with negative (vanishing) parts avoids the presence of singularities on the real axis of the $\eta$ plane.

In particular we note that the Laplace transform of $E_z^i$ (1) at $y = 0$ is

$$V_{1+}^i(\eta) = \int_0^\infty E_z^i(x,0) e^{j\eta\, x} dx = \frac{jE_o}{\eta - \eta_o} \tag{8}$$

with a pole singularity $\eta_o = -k\cos(\varphi_o)$ whose location in $\eta$ complex plane depends on the incident angle $\varphi_o$ (i.e. $\eta_o$ is in the 2nd or 4th quadrant along the segment that connects $k$ to $-k$).

In order to model layered regions we also define the Fourier transforms

$$\begin{cases} v(\eta, y) = \int\limits_{-\infty}^{\infty} E_z(x, y) e^{j\eta\, x} dx \\ i(\eta, y) = \int\limits_{-\infty}^{\infty} H_x(x, y) e^{j\eta\, x} dx \end{cases} \tag{9}$$

that are related to the Laplace transforms at the interfaces $y = 0, x > 0$ and $y = -d, x < s$ respectively via

$$\begin{cases} v(\eta, y = 0_-) = v(\eta, y = 0_+) = V_{1+}(\eta) + V_{1\pi+}(-\eta) = V_{1+}(\eta) \\ i(\eta, y = 0_-) = I_{1+}(\eta) - I_{1\pi+}(-\eta) \\ i(\eta, y = 0_+) = I_{1+}(\eta) + I_{a-}(\eta) \end{cases} \tag{10}$$

and

$$\begin{cases} v(\eta, y = -d_+) = v(\eta, y = -d_-) = e^{j\eta s} V_{2+}(\eta) + e^{j\eta s} V_{2\pi+}(-\eta) = e^{j\eta s} V_{2\pi+}(-\eta) \\ i(\eta, y = -d_+) = e^{j\eta s} I_{2+}(\eta) - e^{j\eta s} I_{2\pi+}(-\eta) \\ i(\eta, y = -d_-) = e^{j\eta s} I_{d+}(\eta) - e^{j\eta s} I_{2\pi+}(-\eta) \end{cases} \tag{11}$$

Note that the PEC boundary conditions enforce $V_{1\pi+}(-\eta) = V_{a-}(\eta) = 0$ and $V_{2+}(\eta) = V_{d+}(\eta) = 0$ because $E_z = 0$ on the two sides of PEC half-planes. In the following to determine the matrix Wiener-Hopf equations we make extensive reference to the quantities (4)-(7) labeled axial spectral unknowns: the voltages $V$ are related to $E_z$ and the currents $I$ are related to $H_x$.

From Maxwell's equations, the use of transverse field equations [16],[17] for planar stratified regions at $E_z$ polarization in spectral domain allows to model the three regions using transmission line modelling in terms of Fourier transforms (9):

$$\begin{cases} -\frac{dv(\eta,y)}{dx} = j\xi(\eta) Z_\infty(\eta) i(\eta, y) \\ -\frac{di(\eta,y)}{dx} = j\xi(\eta) Y_\infty(\eta) v(\eta, y) \end{cases} \tag{12}$$

where $\xi(\eta) = \sqrt{k^2 - \eta^2}$ is the spectral propagation constant and $Z_\infty(\eta) = 1/Y_\infty(\eta) = kZ_o/\xi(\eta)$ is the spectral characteristic impedance of the transmission line along $y$ for $TE_y$ ($H_y$) modes ($Z_o = 1/Y_o$ is the free space impendence).

The properties of the transmission line modelling for the three regions allows to obtain the matrix Wiener-Hopf equations by reframing the Fourier transforms unknowns into Laplace transforms unknowns.

Thus, the application of Fredholm factorization [15]-[16] allows to obtain integral representations that relates current and voltage unknowns by eliminating some of the unknowns and it allows to obtain Fredholm integral equations of second kind for the solution of the problem.

In the following section we examine each regions starting from the Wiener-Hopf equations to obtain the relevant integral representations by contour integration. In particular we will use the contours $\gamma_{1\eta}$ and $\gamma_{2\eta}$ that are respectively the *smile* and the *frown* integration line in $\eta$-plane [15]-[16], i.e. the real axis of the $\eta'$-plane indented at $\eta' = \eta$ with a small semi-circumference respectively in the lower half plane and in the upper half plane.

The application of Fredholm factorization is based on integral decomposition of the Wiener-Hopf unknowns. The classical decomposition equations (see Ch. 3 of [16]) apply to conventional (or standard) plus functions. Non-standard functions present poles located in the standard conventional regular half-plane that is $\mathrm{Im}[\eta] \geq 0$ for the plus functions $F_+(\eta)$ and $\mathrm{Im}[\eta] \leq 0$ for the minus functions $F_-(\eta)$. The presence of not standard poles modifies the Cauchy decompositions formula as following:

$$\begin{array}{ll} \frac{1}{2\pi j}\int\limits_{\gamma_{1\eta}} \frac{F_+(\eta')}{\eta'-\eta}d\eta' = F_+(\eta) - F_+^{n.s.}(\eta), & \frac{1}{2\pi j}\int\limits_{\gamma_{2\eta}} \frac{F_+(\eta')}{\eta'-\eta}d\eta' = -F_+^{n.s.}(\eta) \\ \frac{1}{2\pi j}\int\limits_{\gamma_{2\eta}} \frac{F_-(\eta')}{\eta'-\eta}d\eta' = -F_-(\eta) + F_-^{n.s.}(\eta), & \frac{1}{2\pi j}\int\limits_{\gamma_{1\eta}} \frac{F_-(\eta')}{\eta'-\eta}d\eta' = F_-^{n.s.}(\eta) \end{array} \tag{13}$$

for $\eta \in \mathbb{R}$ and where $F_+^{n.s.}(\eta)$ and $F_-^{n.s.}(\eta)$ are the not standard part of $F_+(\eta)$ and $F_-(\eta)$. To demonstrate this result, we recall that $\int\limits_{\Gamma_{1\eta}} \frac{F_+(\eta')}{\eta'-\eta}d\eta' \to 0$ ($\int\limits_{\Gamma_{2\eta}} \frac{F_-(\eta')}{\eta'-\eta}d\eta' \to 0$) where $\Gamma_{1\eta}$ ($\Gamma_{2\eta}$) is the half-circle with radius $|\eta| \to \infty$ in the upper (lower) $\eta$ half-plane.

We recall that (13) hold for $\eta \in \mathbb{R}$. From here on this assumption is valid unless otherwise specified. Another important assumption is that, while computing $\xi(\eta)$, we consider branch cuts compatible with the mathematical procedure that

will be proposed in next sections, since it is based on contour warping of the integration line: for instance we can assume as branch line of $\xi$ the classical line $Im[\xi(\eta)] = 0$ or the vertical line ($Re[\eta] = Re[k]$, $Im[\eta] < Im[k]$).

## 3. Wiener-Hopf and Integral Representations of the Problem

In this section we examine each regions deriving the relevant Wiener-Hopf equations from the transmission line equations (12). For each region we also obtain the integral representations by contour integration, that are amenable of network interpretation in terms of spectral unknowns.

### *3.1. Region 1: the upper half-space*

Region 1 ($y > 0$) is modelled with an indefinite transmission line along positive $y$ with a port at $y = 0$ labeled port 1, thus from (12) we obtain

$$i(\eta, 0_+) = Y_\infty(\eta) v(\eta, 0_+) \tag{14}$$

i.e. in terms of Laplace transforms

$$I_{a-}(\eta) + I_{1+}(\eta) = Y_\infty(\eta) V_{1+}(\eta) \tag{15}$$

that is the scalar Wiener-Hopf equation that relates current and voltage unknowns in region 1.

Applying the smile $\gamma_{1\eta}$ integration to the first member of (15) and closing the contour with $\Gamma_{1\eta}$ we obtain

$$\frac{1}{2\pi j} \int\limits_{\gamma_{1\eta}} \frac{I_{a-}(\eta) + I_{1+}(\eta)}{\eta' - \eta} d\eta' = I_{1+}(\eta) - I_{1+}^{n.s.}(\eta) + I_{a-}^{n.s}(\eta) \tag{16}$$

The application of the top right formula of (13) to the second member of (15) it yields

$$\begin{aligned} &\tfrac{1}{2\pi j} \int\limits_{\gamma_{1\eta}} \tfrac{Y_\infty(\eta') V_{1+}(\eta')}{\eta' - \eta} d\eta' = \\ &= \tfrac{1}{2\pi j} \int\limits_{\gamma_{1\eta}} \tfrac{Y_\infty(\eta') V_{1+}(\eta')}{\eta' - \eta} d\eta' - \tfrac{1}{2\pi j} \int\limits_{\gamma_{2\eta}} \tfrac{Y_\infty(\eta) V_{1+}(\eta')}{\eta' - \eta} d\eta' - Y_\infty(\eta) V_{1+}^{n.s.}(\eta) \end{aligned} \tag{17}$$

Note that in (17)

$$\begin{aligned}&\tfrac{1}{2\pi j}\int\limits_{\gamma_{1\eta}}\tfrac{Y_\infty(\eta')V_{1+}(\eta')}{\eta'-\eta}d\eta'-\tfrac{1}{2\pi j}\int\limits_{\gamma_{2\eta}}\tfrac{Y_\infty(\eta)V_{1+}(\eta')}{\eta'-\eta}d\eta'=\\&=Y_\infty(\eta)V_{1+}(\eta)+\tfrac{1}{2\pi j}\int\limits_{+\infty}^{-\infty}\tfrac{(Y_\infty(\eta')-Y_\infty(\eta))V_{1+}(\eta')}{\eta'-\eta}d\eta'\end{aligned}\tag{18}$$

therefore because of (15) we equate (16) to (17) with the help of (18) obtaining

$$I_{1+}(\eta)=Y_\infty(\eta)V_{1+}(\eta)+\frac{1}{2\pi j}\int\limits_{-\infty}^{\infty}\frac{(Y_\infty(\eta')-Y_\infty(\eta))V_{1+}(\eta')}{\eta'-\eta}d\eta'-I_{sca}(\eta)\tag{19}$$

where $I_{sca}(\eta)=Y_\infty(\eta)V_{1+}^{n.s.\cdot}(\eta)-I_{1+}^{n.s.\cdot}(\eta)+I_{a-}^{n.s}(\eta)$. We note that $I_{sca}(\eta)$ is defined in terms of the non standard singularities of the spectral unknowns that are related to the physical source of the problem. In case of source constituted of an incident plane wave, the singularities of the spectra are poles associated to the GO component of the fields. In this case, the non-standard components of the unknowns can be obtained from GO consideration and using the Laplace transform:

$$\begin{aligned}V_{1+}^{n.s.\cdot}(\eta)&=\tfrac{jE_o(1-e^{-j2dk\sin(\varphi_o)})}{\eta-\eta_o}u(\pi/2-\varphi_o)\\I_{1+}^{n.s.\cdot}(\eta)&=\tfrac{-jY_oE_o\sin(\varphi_o)(1-e^{-j2dk\sin(\varphi_o)})}{\eta-\eta_o}u(\pi/2-\varphi_o)\\I_{a-}^{n.s}(\eta)&=\tfrac{2jY_oE_o\sin(\varphi_o)}{\eta-\eta_o}u(\varphi_o-\pi/2)\end{aligned}\tag{20}$$

where $u(t)$ is unit-step function. We observe that non-standard plus (minus) components are generated for $0<\varphi_o<\pi/2$ ($\pi/2<\varphi_o<\pi$).

Note that (19) can be interpreted as the constitutive equation of Norton type of an equivalent electric network. The equation relates the current $I_{1+}(\eta)$ to the voltage $V_{1+}(\eta)$ through the algebraic-integral admittance operator $\mathcal{Y}_a[\cdot]$ and the short circuit (known) current $I_{sca}(\eta)$:

$$I_{1+}(\eta)=\mathcal{Y}_a[V_{1+}(\eta)]-I_{sca}(\eta)\tag{21}$$

for real $\eta$ and where

$$\mathcal{Y}_a[V_{1+}(\eta)]=Y_\infty(\eta)V_{1+}(\eta)+\frac{1}{2\pi j}\int\limits_{-\infty}^{\infty}y_a(\eta,\eta')V_{1+}(\eta')d\eta'\tag{22}$$

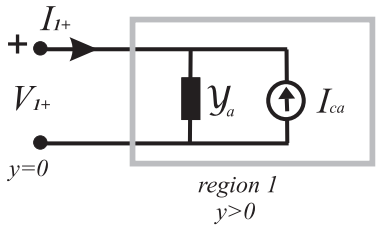


Figure 3: Norton equivalent circuit of region 1 corresponding to (21).

with

$$y_a(\eta, \eta') = \frac{Y_\infty(\eta') - Y_\infty(\eta)}{\eta' - \eta} \tag{23}$$

The final representation of region 1 is therefore the Norton equation (21), see Fig.3, where the input port is port 1 located at $y = 0$ and the box represents the indefinite half-space region effect ($y > d$).

### *3.2. Region 2: the intermediate layer*

Region 2 ($-d < y < 0$) is modelled with a section of transmission line along positive y of length $d$ with two port located at $y = 0$ and $y = -d$ and respectively labeled port 1 and 2. Starting again from (12), by applying the transmission line theory, we obtain the two port representation

$$\begin{cases} i(\eta, 0_-) = -Y_{11}(\eta)v(\eta, 0) - Y_{12}(\eta)v(\eta, -d) \\ i(\eta, -d_+) = Y_{21}(\eta)v(\eta, 0) + Y_{22}(\eta)v(\eta, -d) \end{cases} \tag{24}$$

where

$$\begin{aligned} Y_{11}(\eta) = Y_{22}(\eta) = Y_l(\eta) = -jY_\infty(\eta)\cot[\xi(\eta)d] \\ Y_{12}(\eta) = Y_{21}(\eta) = Y_m(\eta) = j\frac{Y_\infty(\eta)}{\sin[\xi(\eta)d]} \end{aligned} \tag{25}$$

In terms of Laplace transforms by using (10) and (11) the equations (24) become

$$\begin{cases} -I_{1+}(\eta) + I_{1\pi+}(-\eta) = Y_{11}(\eta)[V_{1+}(\eta) + V_{1\pi+}(-\eta)] + Y_{12}(\eta)e^{j\eta s}[V_{2+}(\eta) + V_{2\pi+}(-\eta)] \\ I_{2+}(\eta) - I_{2\pi+}(-\eta) = Y_{21}(\eta)e^{-j\eta s}[V_{1+}(\eta) + V_{1\pi+}(-\eta)] + Y_{22}(\eta)[V_{2+}(\eta) + V_{2\pi+}(-\eta)] \end{cases} \tag{26}$$

These are two Wiener-Hopf equations that relates current and voltage unknowns of the two ports. Because of the regularity properties of WH unknowns we

double the equations (26) by interchanging $\eta$ with $-\eta$:

$$\begin{cases} -I_{1+}(-\eta) + I_{1\pi+}(\eta) = Y_{11}(\eta)[V_{1+}(-\eta) + V_{1\pi+}(\eta)] + Y_{12}(\eta)e^{-j\eta s}[V_{2+}(-\eta) + V_{2\pi+}(\eta)] \\ I_{2+}(-\eta) - I_{2\pi+}(\eta) = Y_{21}(\eta)e^{j\eta s}[V_{1+}(-\eta) + V_{1\pi+}(\eta)] + Y_{22}(\eta)[V_{2+}(-\eta) + V_{2\pi+}(\eta)] \end{cases} \tag{27}$$

Taking into account the 1st equation of (26) and the 2nd equation of (27) we eliminate respectively the unknowns $I_{1\pi+}(-\eta)$ and $I_{2+}(-\eta)$ by contour integration and using (13).

By applying the smile $\gamma_{1\eta}$ integration to the left-hand side (LHS) of the 1st eq in (26) and closing the contour with $\Gamma_{1\eta}$ we obtain

$$\frac{1}{2\pi j}\int\limits_{\gamma_{1\eta}} \frac{-I_{1+}(\eta') + I_{1\pi+}(-\eta')}{\eta' - \eta} d\eta' = -I_{1+}(\eta) + I_{1+}^{n.s.\cdot}(\eta) + I_{1\pi+}^{n.s}(-\eta) \tag{28}$$

where $I_{1\pi+}^{n.s.\cdot}(-\eta) = 0$ since it is the Laplace transform of a GO component with finite support (i.e. entire function). Repeating the $\gamma_{1\eta}$ integration on the right-hand side (RHS) of the 1st eq in (26), it yields

$$\begin{aligned} &\tfrac{1}{2\pi j}\int\limits_{\gamma_{1\eta}} \tfrac{Y_{11}(\eta')V_{1+}(\eta') + Y_{12}(\eta')e^{j\eta' s}V_{2\pi+}(-\eta')}{\eta' - \eta} d\eta' = \\ &= \tfrac{1}{2\pi j}\int\limits_{\gamma_{1\eta}} \tfrac{Y_{11}(\eta')V_{1+}(\eta')}{\eta' - \eta} d\eta' - \tfrac{1}{2\pi j}\int\limits_{\gamma_{2\eta}} \tfrac{Y_{11}(\eta)V_{1+}(\eta')}{\eta' - \eta} d\eta' - Y_{11}(\eta)V_{1+}^{n.s.\cdot}(\eta) + \\ &+ \tfrac{1}{2\pi j}\int\limits_{\gamma_{1\eta}} \tfrac{Y_{12}(\eta')e^{j\eta' s}V_{2\pi+}(-\eta')}{\eta' - \eta} d\eta' - \tfrac{1}{2\pi j}\int\limits_{\gamma_{1\eta}} \tfrac{Y_{12}(\eta)e^{j\eta s}V_{2\pi+}(-\eta')}{\eta' - \eta} d\eta' \end{aligned} \tag{29}$$

where we have used the following properties

$$\begin{aligned} &\tfrac{1}{2\pi j}\int\limits_{\gamma_{2\eta}} \tfrac{Y_{11}(\eta)V_{1+}(\eta')}{\eta' - \eta} d\eta' = -Y_{11}(\eta)V_{1+}^{n.s.\cdot}(\eta) \\ &\tfrac{1}{2\pi j}\int\limits_{\gamma_{1\eta}} \tfrac{Y_{12}(\eta)e^{j\eta s}V_{2\pi+}(-\eta')}{\eta' - \eta} d\eta' = 0 \end{aligned} \tag{30}$$

derived directly from (13) and the regularity properties of the unknowns, and where $V_{2\pi+}^{n.s.\cdot}(-\eta) = 0$ since it is the Laplace transform of a GO component with finite support (i.e. entire function).

By noting inside (29) that

$$\begin{aligned} &\tfrac{1}{2\pi j}\int\limits_{\gamma_{1\eta}} \tfrac{Y_{11}(\eta')V_{1+}(\eta')}{\eta' - \eta} d\eta' - \tfrac{1}{2\pi j}\int\limits_{\gamma_{2\eta}} \tfrac{Y_{11}(\eta)V_{1+}(\eta')}{\eta' - \eta} d\eta' = \\ &= Y_{11}(\eta)V_{1+}(\eta) + \tfrac{1}{2\pi j}\int\limits_{-\infty}^{\infty} \tfrac{(Y_{11}(\eta') - Y_{11}(\eta))V_{1+}(\eta')}{\eta' - \eta} \end{aligned} \tag{31}$$

and

$$\begin{aligned}&\tfrac{1}{2\pi j}\int\limits_{\gamma_{1\eta}}\tfrac{Y_{12}(\eta')e^{j\eta' s}V_{2\pi+}(-\eta')}{\eta'-\eta}d\eta'-\tfrac{1}{2\pi j}\int\limits_{\gamma_{1\eta}}\tfrac{Y_{12}(\eta)e^{j\eta s}V_{2\pi+}(-\eta')}{\eta'-\eta}d\eta'=\\&=\tfrac{1}{2\pi j}\int\limits_{-\infty}^{\infty}\tfrac{(Y_{12}(\eta)e^{j\eta s}-Y_{12}(\eta')e^{-j\eta' s})V_{2\pi+}(\eta')}{\eta'+\eta}d\eta'\end{aligned}\tag{32}$$

we obtain a regularized version of (29)

$$\begin{aligned}&\tfrac{1}{2\pi j}\int\limits_{\gamma_{1\eta}}\tfrac{Y_{11}(\eta')V_{1+}(\eta')+Y_{12}(\eta')e^{j\eta' s}V_{2\pi+}(-\eta')}{\eta'-\eta}d\eta'=\\&=Y_{11}(\eta)V_{1+}(\eta')+\tfrac{1}{2\pi j}\int\limits_{-\infty}^{\infty}\tfrac{(Y_{11}(\eta')-Y_{11}(\eta))V_{1+}(\eta')}{\eta'-\eta}-Y_{11}(\eta)V_{1+}^{n.s.\cdot}(\eta)+\\&+\tfrac{1}{2\pi j}\int\limits_{-\infty}^{\infty}\tfrac{(Y_{12}(\eta)e^{j\eta s}-Y_{12}(\eta')e^{-j\eta' s})V_{2\pi+}(\eta')}{\eta'+\eta}d\eta'\end{aligned}\tag{33}$$

Equating the RHS of (28) to the RHS of (33) we obtain

$$\begin{aligned}&-I_{1+}(\eta)=+Y_{11}(\eta)V_{1+}(\eta)+\tfrac{1}{2\pi j}\int\limits_{-\infty}^{\infty}\tfrac{(Y_{11}(\eta')-Y_{11}(\eta))V_{1+}(\eta')}{\eta'-\eta}+\\&+\tfrac{1}{2\pi j}\int\limits_{-\infty}^{\infty}\tfrac{(Y_{12}(\eta)e^{j\eta s}-Y_{12}(\eta')e^{-j\eta' s})V_{2\pi+}(\eta')}{\eta'+\eta}d\eta'-I_{scb1}(\eta)\end{aligned}\tag{34}$$

where $I_{scb1}(\eta)=I_{1+}^{n.s.\cdot}(\eta)+Y_{11}(\eta)V_{1+}^{n.s.\cdot}(\eta)$. We note that $I_{scb1}(\eta)$ is defined in terms of non standard singularities of the spectral unknowns that are related to the physical source of the problem, for instance an incident plane wave, see (20). In this case the non-standard plus components are generated only for $0<\varphi_o<\pi/2$.

Eq. (34) is one of the two equations of region 2 that relates the spectral unknown $I_{1+}(\eta)$ to $V_{1+}(\eta)$ and $V_{2\pi+}(\eta)$.

To obtain a 2nd equation for region 2 that relates the unknown $I_{2\pi+}(\eta)$ to $V_{1+}(\eta)$ and $V_{2\pi+}(\eta)$, we start by considering the 2nd eq. of (27). Similar to the 1st equation, we apply the smile $\gamma_{1\eta}$ integration to the LHS of the 2nd eq in (27) and closing the contour with $\Gamma_{1\eta}$ we obtain

$$\frac{1}{2\pi j}\int\limits_{\gamma_{1\eta}}\frac{I_{2+}(-\eta')-I_{2\pi+}(\eta')}{\eta'-\eta}d\eta'=I_{2+}^{n.s}(-\eta)-I_{2\pi+}(\eta)+I_{2\pi+}^{n.s}(\eta)\tag{35}$$

where $I_{2\pi+}^{n.s.}(\eta)=0$.

Repeating the $\gamma_{1\eta}$ integration on the right-hand side (RHS) of the 1st eq in

(27), it yields

$$\begin{aligned}
&\tfrac{1}{2\pi j}\int\limits_{\gamma_{1\eta}} \tfrac{Y_{21}(\eta')e^{j\eta' s}V_{1+}(-\eta')+Y_{22}(\eta')V_{2\pi+}(\eta')}{\eta'-\eta}d\eta' = \\
&= \tfrac{1}{2\pi j}\int\limits_{\gamma_{1\eta}} \tfrac{Y_{22}(\eta')V_{2\pi+}(\eta')}{\eta'-\eta}d\eta' - \tfrac{1}{2\pi j}\int\limits_{\gamma_{2\eta}} \tfrac{Y_{22}(\eta)V_{2\pi+}(\eta)}{\eta'-\eta}d\eta' + \\
&+ \tfrac{1}{2\pi j}\int\limits_{\gamma_{1\eta}} \tfrac{Y_{21}(\eta')e^{j\eta' s}V_{1+}(-\eta')}{\eta'-\eta}d\eta' - \tfrac{1}{2\pi j}\int\limits_{\gamma_{1\eta}} \tfrac{Y_{21}(\eta)e^{j\eta s}V_{1+}(-\eta')}{\eta'-\eta}d\eta' + \\
&+ Y_{21}(\eta)e^{j\eta s}V_{1+}^{n.s.\cdot}(-\eta)
\end{aligned} \tag{36}$$

where we have used the following properties

$$\begin{aligned}
&\tfrac{1}{2\pi j}\int\limits_{\gamma_{2\eta}} \tfrac{Y_{22}(\eta)V_{2\pi+}(\eta')}{\eta'-\eta}d\eta' = 0 \\
&\tfrac{1}{2\pi j}\int\limits_{\gamma_{1\eta}} \tfrac{Y_{21}(\eta)e^{j\eta s}V_{1+}(-\eta')}{\eta'-\eta}d\eta' = Y_{21}(\eta)\mathrm{e}^{j\eta s}V_{1+}^{n.s.\cdot}(-\eta)
\end{aligned} \tag{37}$$

where $V_{2\pi+}^{n.s.\cdot}(-\eta) = 0$.

By noting inside (36) that

$$\begin{aligned}
&\tfrac{1}{2\pi j}\int\limits_{\gamma_{1\eta}} \tfrac{Y_{22}(\eta')V_{2\pi+}(\eta')}{\eta'-\eta}d\eta' - \tfrac{1}{2\pi j}\int\limits_{\gamma_{2\eta}} \tfrac{Y_{22}(\eta)V_{2\pi+}(\eta')}{\eta'-\eta}d\eta' = \\
&= Y_{22}(\eta)V_{2\pi+}(\eta) + \tfrac{1}{2\pi j}\int\limits_{-\infty}^{\infty} \tfrac{(Y_{22}(\eta')-Y_{22}(\eta))V_{2\pi+}(\eta')}{\eta'-\eta}
\end{aligned} \tag{38}$$

and

$$\begin{aligned}
&\tfrac{1}{2\pi j}\int\limits_{\gamma_{1\eta}} \tfrac{Y_{21}(\eta')e^{j\eta' s}V_{1+}(-\eta')}{\eta'-\eta}d\eta' - \tfrac{1}{2\pi j}\int\limits_{\gamma_{1\eta}} \tfrac{Y_{21}(\eta)e^{j\eta s}V_{1+}(-\eta')}{\eta'-\eta}d\eta' = \\
&= \tfrac{1}{2\pi j}\int\limits_{-\infty}^{\infty} \tfrac{(Y_{21}(\eta)e^{j\eta s}-Y_{21}(\eta')e^{-j\eta' s})V_{1+}(\eta')}{\eta'+\eta}d\eta'
\end{aligned} \tag{39}$$

we obtain a regularized version of (36)

$$\begin{aligned}
&\tfrac{1}{2\pi j}\int\limits_{\gamma_{1\eta}} \tfrac{Y_{21}(\eta')e^{j\eta' s}V_{1+}(-\eta')+Y_{22}(\eta')V_{2\pi+}(\eta')}{\eta'-\eta}d\eta' = \\
&= Y_{22}(\eta)V_{2\pi+}(\eta') + \tfrac{1}{2\pi j}\int\limits_{-\infty}^{\infty} \tfrac{(Y_{22}(\eta')-Y_{22}(\eta))V_{2\pi+}(\eta')}{\eta'-\eta} + \\
&\tfrac{1}{2\pi j}\int\limits_{-\infty}^{\infty} \tfrac{(Y_{21}(\eta)e^{j\eta s}-Y_{21}(\eta')e^{-j\eta' s})V_{1+}(\eta')}{\eta'+\eta}d\eta' + \\
&+ Y_{21}(\eta)e^{j\eta s}V_{1+}^{n.s.\cdot}(-\eta)
\end{aligned} \tag{40}$$

Equating the RHS of (35) to the RHS of (40) we obtain

$$\begin{aligned}
&-I_{2\pi+}(\eta) = Y_{22}(\eta)V_{2\pi+}(\eta) + \tfrac{1}{2\pi j}\int\limits_{-\infty}^{\infty} \tfrac{(Y_{22}(\eta')-Y_{22}(\eta))V_{2\pi+}(\eta')}{\eta'-\eta} + \\
&\tfrac{1}{2\pi j}\int\limits_{-\infty}^{\infty} \tfrac{(Y_{21}(\eta)e^{j\eta s}-Y_{21}(\eta')e^{-j\eta' s})V_{1+}(\eta')}{\eta'+\eta}d\eta' - I_{scb2}(\eta)
\end{aligned} \tag{41}$$

where $I_{scb2}(\eta) = I_{2+}^{n.s}(-\eta) - Y_{21}(\eta)e^{j\eta s}V_{1+}^{n.s.}(-\eta)$. We note that $I_{scb2}(\eta)$ is defined in terms of non standard plus singularities that are related to the physical source of the problem. For a plane wave source (see (20)) we have

$$I_{2+}^{n.s.}(\eta) = \frac{-2jY_oE_o\sin(\varphi_o)(e^{-jk(-s\cos(\varphi_o)+d\sin(\varphi_o))})}{\eta-\eta_o}u(\pi/2-\varphi_o) \tag{42}$$

thus $I_{scb2}(\eta)$ is non null only for $0 < \varphi_o < \pi/2$.

Eq. (41) is the second equation of region 2. in particular it relates the spectral unknown $I_{2\pi+}(\eta)$ to $V_{1+}(\eta)$ and $V_{2\pi+}(\eta)$.

Eqs. (34) and (41) can be interpreted as the constitutive equations of Norton type of an equivalent electric two-port network, where the input ports are port 1 located at $y = 0$ and port 2 located at $y = -d$. In particular they relates the currents of the two ports $I_{1+}(\eta)$ and $I_{2\pi+}(\eta)$ to the voltages $V_{1+}(\eta)$ and $V_{2\pi+}(\eta)$ through a matrix algebraic-integral admittance operator $\underline{\underline{\mathcal{Y}_{\mathbf{b}}}}[\cdot]$ and short circuit (known) vector currents $\mathbf{I_{scb}}(\eta)$:

$$\begin{pmatrix} -I_{1+}(\eta) \\ -I_{2\pi+}(\eta) \end{pmatrix} = \begin{bmatrix} \mathcal{Y}_{b11}[V_{1+}(\eta)] & \mathcal{Y}_{b12}[V_{2\pi+}(\eta)] \\ \mathcal{Y}_{b21}[V_{1+}(\eta)] & \mathcal{Y}_{b22}[V_{2\pi+}(\eta)] \end{bmatrix} - \begin{pmatrix} I_{scb1}(\eta) \\ I_{scb2}(\eta) \end{pmatrix} \tag{43}$$

for real $\eta$ and where

$$\begin{aligned}
\mathcal{Y}_{b11}[V_{1+}(\eta)] &= Y_{11}(\eta)V_{1+}(\eta) + \tfrac{1}{2\pi j}\int_{-\infty}^{\infty} y_{b11}(\eta,\eta')V_{1+}(\eta')d\eta' \\
\mathcal{Y}_{b12}[V_{2\pi+}(\eta)] &= \tfrac{1}{2\pi j}\int_{-\infty}^{\infty} y_{b12}(\eta,\eta')V_{2\pi+}(\eta')d\eta' \\
\mathcal{Y}_{b21}[V_{1+}(\eta)] &= \tfrac{1}{2\pi j}\int_{-\infty}^{\infty} y_{b21}(\eta,\eta')V_{1+}(\eta')d\eta' \\
\mathcal{Y}_{b22}[V_{2\pi+}(\eta)] &= Y_{22}(\eta)V_{2\pi+}(\eta) + \tfrac{1}{2\pi j}\int_{-\infty}^{\infty} y_{b22}(\eta,\eta')V_{2\pi+}(\eta')d\eta'
\end{aligned} \tag{44}$$

with

$$\begin{aligned}
y_{b11}(\eta,\eta') &= \tfrac{Y_{11}(\eta')-Y_{11}(\eta)}{\eta'-\eta} & y_{b12}(\eta,\eta') &= \tfrac{(Y_{12}(\eta)\mathrm{e}^{j\eta s}-Y_{12}(\eta')\mathrm{e}^{-j\eta' s})}{\eta'+\eta} \\
y_{b21}(\eta,\eta') &= \tfrac{(Y_{21}(\eta)\mathrm{e}^{j\eta s}-Y_{21}(\eta')\mathrm{e}^{-j\eta' s})}{\eta'+\eta} & y_{b22}(\eta,\eta') &= \tfrac{Y_{22}(\eta')-Y_{22}(\eta)}{\eta'-\eta}
\end{aligned} \tag{45}$$

The final representation of region 2 is therefore the two-port Norton model (43) amenable of network representation, see Fig.4, where the input ports are port 1 located at $y = 0$ and port 2 located at $y = -d$ and the box represents the finite region effect ($-d < y < 0$).

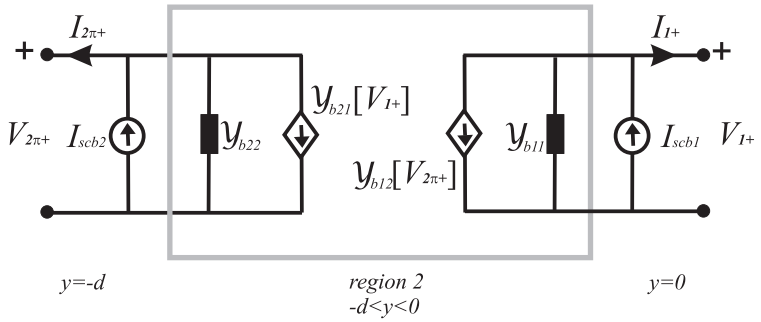


Figure 4: Norton equivalent model of region 2 corresponding to (43).

### *3.3. Region 3: the lower half-space*

Similar to Region 1, region 3 ($y > -d$) is modelled by an indefinite transmission line along $y$ with a port at $y = -d$ labeled port 2, thus from (12) we obtain

$$i(\eta, -d_-) = -Y_\infty(\eta) v(\eta, -d_-) \tag{46}$$

i.e. in terms of Laplace transforms defined in Section 2

$$e^{j\eta s} I_{2-}(\eta) + e^{j\eta s} I_{d+}(\eta) = -e^{j\eta s} Y_\infty(\eta) V_{2-}(\eta) \tag{47}$$

that is the scalar Wiener-Hopf equation that relates current and voltage unknowns. Taking into account that

$$I_{2-}(\eta) = -I_{2\pi+}(-\eta), \quad V_{2-}(\eta) = V_{2\pi+}(-\eta) \tag{48}$$

and interchanging $\eta$ with $-\eta$ we obtain

$$-I_{d+}(-\eta) + I_{2\pi+}(\eta) = Y_\infty(\eta) V_{2\pi+}(\eta) \tag{49}$$

Applying the smile $\gamma_{1\eta}$ integration to the first member of (49) and closing the contour with $\Gamma_{1\eta}$ we obtain

$$\frac{1}{2\pi j} \int\limits_{\gamma_{1\eta}} \frac{-I_{d+}(-\eta) + I_{2\pi+}(\eta)}{\eta' - \eta} d\eta' = I_{2\pi+}(\eta) \tag{50}$$

We apply the $\gamma_{1\eta}$ contour integration to the second member of (49) and due to the regularity of $V_{2\pi+}(\eta)$ (which is an entire function thus $V^{n.s.}_{2\pi+}(\eta) = 0$) we

obtain

$$\frac{1}{2\pi j}\int\limits_{\gamma_{1\eta}}\frac{Y_\infty(\eta')V_{2\pi+}(\eta')}{\eta'-\eta}d\eta' = \frac{1}{2\pi j}\int\limits_{\gamma_{1\eta}}\frac{Y_\infty(\eta')V_{2\pi+}(\eta')}{\eta'-\eta}d\eta' - \frac{1}{2\pi j}\int\limits_{\gamma_{2\eta}}\frac{Y_\infty(\eta)V_{2\pi+}(\eta')}{\eta'-\eta}d\eta' = \\ = Y_\infty(\eta)V_{2\pi+}(\eta) + \frac{1}{2\pi j}\int\limits_{-\infty}^{\infty}\frac{(Y_\infty(\eta')-Y_\infty(\eta))V_{2\pi+}(\eta')}{\eta'-\eta}d\eta' \tag{51}$$

By equating (50) to (51) because of (49) it yields

$$I_{2\pi+}(\eta) = Y_\infty(\eta)V_{2\pi+}(\eta) + \frac{1}{2\pi j}\int_{-\infty}^{\infty}\frac{(Y_\infty(\eta')-Y_\infty(\eta))V_{2\pi+}(\eta')}{\eta'-\eta}d\eta' \tag{52}$$

which is an homogenous equations with respect to the results obtained for region 1 and 2.

Note that also (52) can be interpreted as the constitutive equation of Norton type of an equivalent electric network without short circuit currents therefore in this case we have a one-port admittance representation. The equation relates the current $I_{2\pi+}(\eta)$ to the voltage $V_{2\pi+}(\eta)$ through the algebraic-integral admittance operator $\mathcal{Y}_c[\cdot]$ :

$$I_{2\pi+}(\eta) = \mathcal{Y}_c[V_{2\pi+}(\eta)] \tag{53}$$

for real $\eta$ and where

$$\mathcal{Y}_c[V_{2\pi+}(\eta)] = Y_\infty(\eta)V_{2\pi+}(\eta) + \frac{1}{2\pi j}\int\limits_{-\infty}^{\infty} y_c(\eta,\eta')V_{2\pi+}(\eta')d\eta' \tag{54}$$

with

$$y_c(\eta,\eta') = \frac{Y_\infty(\eta')-Y_\infty(\eta)}{\eta'-\eta} \tag{55}$$

The final representation of region 3 is therefore the Norton model (53), see Fig.5, where the input port is port 2 located at $y=-d$ and the box represents the indefinite half-space region effect ($y<-d$).

## 4. Fredholm factorization and Solution

By considering the integral representations (21), (43), (53) related to the three regions respectively region 1, 2 and 3 and/or by connecting the three

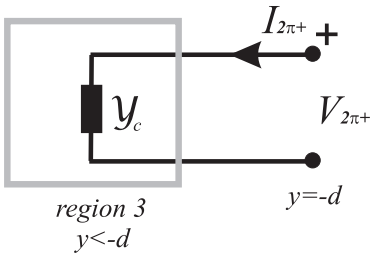


Figure 5: Norton equivalent circuit of region 3 corresponding to (53).

networks representing the regions (Figs. 3-5) we obtain a comprehensive mathematical model of the problem, i.e. a model that considers all the physical interactions of the problem together. By substitution (i.e. by circuital analysis) we eliminate the current unknowns and we obtain a system of two Fredholm integral equations of second kind (FIEs) in normal form with voltage unknowns, i.e. $V_{1+}(\eta)$ and $V_{2\pi+}(\eta)$:

$$\begin{aligned} &V_{1+}(\eta)+\tfrac{1}{2\pi j}\int_{-\infty}^{\infty}\tfrac{(Z_t(\eta)Y_t(\eta')-1)V_{1+}(\eta')}{\eta'-\eta}d\eta'+\tfrac{1}{2\pi j}\int_{-\infty}^{\infty}\tfrac{Z_t(\eta)(Y_{12}(\eta)\mathrm{e}^{j\eta s}-Y_{12}(\eta')\mathrm{e}^{-j\eta' s})V_{2\pi+}(\eta')}{\eta'+\eta}d\eta'=N_1(\eta)\\ &V_{2\pi+}(\eta)+\tfrac{1}{2\pi j}\int_{-\infty}^{\infty}\tfrac{(Z_t(\eta)Y_t(\eta')-1)V_{2\pi+}(\eta')}{\eta'-\eta}d\eta'+\tfrac{1}{2\pi j}\int_{-\infty}^{\infty}\tfrac{Z_t(\eta)(Y_{21}(\eta)\mathrm{e}^{j\eta s}-Y_{21}(\eta')\mathrm{e}^{-j\eta' s})V_{1+}(\eta')}{\eta'+\eta}d\eta'=N_2(\eta)\end{aligned} \tag{56}$$

with real $\eta$ and where

$$Y_t(\eta)=Y_l(\eta)+Y_\infty(\eta)=-j\frac{\xi(\eta)e^{+j\xi(\eta)d}}{kZ_o\sin(\xi(\eta)d)}=\frac{1}{Z_t(\eta)} \tag{57}$$

and

$$\begin{aligned} N_1(\eta)&=Z_t(\eta)(I_{scb1}(\eta)+I_{sca}(\eta))\\ N_2(\eta)&=Z_t(\eta)I_{scb2}(\eta)\end{aligned} \tag{58}$$

and by recalling the definitions reported in (12), (25), (19), (34), (41). Note that (56) show symmetrical algebraic-integral operators $1+P[\cdot]$ and $Q[\cdot]$ applied to $V_{1+}(\eta)$ and $V_{2\pi+}(\eta)$, i.e. we can rewrite the equations as

$$\begin{aligned} (1+P[\cdot])V_{1+}(\eta)+Q[V_{2\pi+}(\eta)]&=N_1(\eta)\\ Q[V_{1+}(\eta)]+(1+P[\cdot])V_{2\pi+}(\eta)&=N_2(\eta)\end{aligned} \tag{59}$$

We observe that (56) constitute a non-singular integral representation with compact kernels [19], in particular it is regular at $\eta=\eta'$. The same equation

holds for a different integration line when the observation points ($\eta$) lie on the integration line ($\eta'$). In particular we consider to warp the the original integration line of (56) (the real axis of $\eta$ plane) into the line $B_\theta = \{\eta(u) = ue^{j\theta}, -\infty < u < \infty\}$ with $0 \leq \theta \leq \pi/2$ that does not capture singularities of the integrand and allows fast convergence because it leaves far away the branch points $\pm k$ of $\xi(\eta)$ because both the singularities and $\pm k$ are located in the 2nd and 4th quadrant of $\eta$ plane. Consequently we rewrite the equation (56) as

$$\begin{aligned} V_{1+}(\eta)+\frac{e^{j\theta}}{2\pi j}\int\limits_{B_\theta}\frac{(Z_t(\eta)Y_t(\eta')-1)V_{1+}(ue^{j\theta})}{ue^{j\theta}-\eta}du+\frac{e^{j\theta}}{2\pi j}\int\limits_{B_\theta}\frac{Z_t(\eta)(Y_{12}(\eta)\mathrm{e}^{j\eta s}-Y_{12}(ue^{j\theta})\mathrm{e}^{-jue^{j\theta}s})V_{2\pi+}(ue^{j\theta})}{ue^{j\theta}+\eta}du=N_1(\eta) \\ V_{2\pi+}(\eta)+\frac{e^{j\theta}}{2\pi j}\int\limits_{B_\theta}\frac{(Z_t(\eta)Y_t(ue^{j\theta})-1)V_{2\pi+}(ue^{j\theta})}{ue^{j\theta}-\eta}du+\frac{e^{j\theta}}{2\pi j}\int\limits_{B_\theta}\frac{Z_t(\eta)(Y_{21}(\eta)\mathrm{e}^{j\eta s}-Y_{21}(ue^{j\theta})\mathrm{e}^{-jue^{j\theta}s})V_{1+}(ue^{j\theta})}{ue^{j\theta}+\eta}du=N_2(\eta) \end{aligned} \tag{60}$$

with $\eta \in B_\theta$.

However, due to the asymptotic properties of kernels in (60) (in particular see $Q[\cdot]$ in (59)) we need to impose the following constraint related to the geometry of the problem

$$\theta < \theta_c = \arctan(d/|s|) \tag{61}$$

Fast convergence of kernels is quickly obtained for any $\theta$ such that $0 << \theta \lesssim \theta_c$.

Fredholm theory guarantees the convergence via numerical procedure of integral equations of second kind [24]. Since the kernels in (60) presents well suited behavior, we use a simple sample and hold quadrature scheme to obtain accurate and stable numerical solutions. We apply uniform sampling $f(h\,i)$ with $i = -\frac{A}{h}..\frac{A}{h}$ and modified left-rectangle numerical integration formula $\int\limits_{-\infty}^{\infty} f(u)du \approx h \sum\limits_{i=-A/h}^{A/h} f(h\,i)$ where $A$ and $h$ are respectively the truncation parameter and the step parameter for the integrals in $u$. The total number of samples is $N = 2A/h + 1$. This rule has been successfully applied in wedge problems [25]-[27], [19]-[20]. We observe that as $A \to +\infty$ and $h \to 0$, the numerical solution of the FIEs converges to the exact solution [24]; consequently $h$ has to be chosen as small as possible and $A$ has to be chosen as large as possible. In practical numerical implementations $A$ and $h$ are finite and they are selected according to the kernel behavior (spectral bandwidth and shape).

In our computational tests we have considered integration contours $B_\theta$ with

a maximum $\theta$ equal to $\pi/4$. This selection allows to get a good convergence rate in the numerical discretization of (60). We also note that the constraint (61) can be relaxed while truncating the original infinite interval of integration since the truncated interval make the kernels automatically compact.

The discretization procedure yields a linear systems whose unknown vector is constituted of samples of $V_{1+}(\eta)$ and $V_{2\pi+}(\eta)$ along $B_\theta$ in the interval $u \in [-A, A]$ with step $h$. Finally we reconstruct $V_{1+}(\eta)$ by using the discretized version of (60). In order to obtain the currents $I_{1+}(\eta)$ and $I_{2\pi+}(\eta)$ we resorts to the discretized version of integral representations (21), (53) or (43) that produce same results.

## 5. Estimation of Physical/Engineering Quantities

In this section, with reference to Fig. 1, we illustrate how to compute the GTD/UTD diffraction coefficients and the total far fields in region 1 and 3, and the transmitted scattered energy flux from region 1 to region 3, while the source is constituted of an $E_z$ polarized plane wave.

### *5.1. Total far-field in region 1*

According to the transmission line theory (12) for indefinite transmission line and the equivalence theorem, see [16] in particular Ch. 7, the Fourier transform of the total field $E_z(x, y)$ in region 1 ($y > 0$) is given by

$$v(\eta, y) = v^p(\eta, y) + v^m(\eta, y) = v^p(\eta, y) + v^m(\eta, 0)e^{-j\xi y} \tag{62}$$

In (62) $v^p(\eta, y)$ is the Fourier transform of the GO primary field

$$E_z^p(x, y) = E_z^i(x, y) + E_z^{pr1}(x, y) \tag{63}$$

that is the superposition of the incident wave $E_z^i(x, y)$ and the reflected wave $E_z^{pr1}(x, y)$ in presence of a PEC plane at $y = 0$. In the following we will use also the reflected wave $E_z^{pr2}(x, y)$ in presence of just a PEC plane at $y = -d$. Note that similarly to (8) $v^p(\eta, 0)$ is a function with a pole at $\eta_o$. In the same equation

$v^m(\eta, y)$ is the contribution of equivalent magnetic current on the support of the aperture ($x > 0, y = 0$) necessary to fulfill the equivalence theorem in region 1 for the original problem, where

$$v^m(\eta, 0) = v(\eta, 0) = V_{1+}(\eta) \tag{64}$$

since $v^p(\eta, 0) = 0$ because of the PEC boundary condition in the equivalent problem.

The application of inverse Fourier transform to (62) allows to evaluate the total field in any point of region 1

$$E_z(x, y) = E_z^p(x, y) + E_z^m(x, y) \tag{65}$$

with the generalized inverse Fourier transform

$$E_z^m(x, y) = \frac{1}{2\pi} \int_{B_+} V_{1+}(\eta) e^{-j\xi(\eta)y} e^{-j\eta\, x} d\eta \tag{66}$$

where $B_+$ is a horizontal line located above the pole singularity of $V_{1+}(\eta)$, i.e. $\eta_o = -k \cos\varphi_o$.

We note that $E_z^m(x, y)$ includes the diffracted field and the portion of GO field that corrects the primary field $E_z^p(x, y)$ into the correct GO field $E_z^{go}(x, y)$ in region 1 of the original problem. Note that $E_z^{go}(x, y)$ is constituted of: 1) the incident wave $E_z^i(x, y)$, 2) the reflected wave from the upper half-plane $E_z^{r1}(x, y)$ and the reflected wave from the lower half-plane $E_z^{r2}(x, y)$.

We recall that the spectral singularities of the integrand are: the pole $\eta_o$ and the branch points $\pm k$.

The use of polar coordinates $(\rho, \varphi)$ with origin $(x, y) = (0, 0)$ and the application of the steepest descent path (SDP) method [17] to (66) (we apply the Cauchy theorem by closing $B_+$ with the SDP line) it yields

$$E_z^m(\rho, \varphi) = -E_z^{SPD}(\rho, \varphi) + \left[-E_z^{pr1}(\rho, \varphi) + E_z^{pr2}(\rho, \varphi)\right] u(\cos(\varphi) + \cos(\varphi_o)) \tag{67}$$

In (67) $E_z^{SPD}(\rho, \varphi)$ is the contribution of the line integral along the SDP approximated as

$$-E_z^{SPD}(\rho, \varphi) = E_z^d(\rho, \varphi) = E_o \frac{e^{-j(k\rho + \pi/4)}}{\sqrt{2\pi k\rho}} D_1(\varphi, \varphi_o) \tag{68}$$

given in terms of the GTD diffraction coefficient in region 1

$$D_1(\varphi,\varphi_o)=\frac{kv(k\cos\varphi,0)\sin\varphi}{jE_o}=\frac{kV_{1+}(k\cos\varphi)\sin\varphi}{jE_o} \tag{69}$$

Furthermore the extra terms appearing in (67) are due to evaluation of the residue at $\eta=\eta_o$ that depends on the locations of: the SDP path, the saddle point $\eta_s=k\cos\varphi$ and the spectral singularities of $V_{1+}(\eta)$ (the pole $\eta_o$ and the branch point $k$). Since the SDP position depends on the observation direction $\varphi$, while closing the contour integration, the pole $\eta_o$ is captured only for particular directions. In fact varying $\varphi$ the SDP can cross the pole $\eta_o$. This property generates the step functions in (67). Finally, the residue of $\eta_o$ gives the reflected waves $E_z^{pr1}(\rho,\varphi)$ and $E_z^{pr2}(\rho,\varphi)$).

In general, the GO components of the original problem $E_z^{go}(\rho,\varphi)$ and of the equivalent problem $E_z^{p}(\rho,\varphi)$ can be obtained via the residue theorem or via classical GO considerations. In the last case, in region 1 of the original problem, we need to consider that the polar reference system is centered in $(x,y)=(0,0)$, thus for each scattered GO ray (reflected from upper half-plane and reflected from lower half-plane) we need to take into account the different propagation paths with phase and attenuation corrections with respect to the incident field.

Finally from (65) and (67) the total field in region 1 is:

$$\begin{aligned}E_z(x,y)&=E_z^i(\rho,\varphi)+E_z^d(\rho,\varphi)+\\&+E_z^{pr1}(\rho,\varphi)u(-\cos(\varphi)-\cos(\varphi_o))+E_z^{pr2}(\rho,\varphi)u(\cos(\varphi)+\cos(\varphi_o))\end{aligned} \tag{70}$$

where $E_z^d(\rho,\varphi)$ (68) is the GTD cylindrical wave field, $E_z^{go}(\rho,\varphi)=E_z(\rho,\varphi)-E_z^d(\rho,\varphi)$ is the GO field of the original problem and $E_z(\rho,\varphi)-E_z^i(\rho,\varphi)-E_z^d(\rho,\varphi)=E_z^{r1}(\rho,\varphi)+E_z^{r2}(\rho,\varphi)$ is the combination of the reflected waves of the original problem.

$$\begin{aligned}E_z^{r1}(\rho,\varphi)&=E_z^{pr1}(\rho,\varphi)u(-\cos(\varphi)-\cos(\varphi_o))\\E_z^{r2}(\rho,\varphi)&=E_z^{pr2}(\rho,\varphi)u(\cos(\varphi)+\cos(\varphi_o))\end{aligned} \tag{71}$$

We recall that $E_z^{pr1}(\rho,\varphi)$ and $E_z^{pr2}(\rho,\varphi)$ are the reflected waves of $E_z^i(\rho,\varphi)$ in presence respectively of a PEC plane at $y=0$ and $y=-d$. Both reflected

waves of the original problem (71) have same shadow boundary at $\pi - \varphi_o$ but supplementary angular support in region 1.

In general the GTD $E_z^d(\rho, \varphi)$ is based on the ray concept and, therefore, fails at caustics of rays as at the GO shadow boundaries where GTD diffraction coefficients (69) show infinity [32]. For practical engineering/physical applications, uniform expressions are obtained through the Uniform Theory of Diffraction (UTD) [22]:

$$E_z^{utd}(\rho, \varphi) = E_0 \frac{e^{-j\left(k\rho + \frac{\pi}{4}\right)}}{\sqrt{2\pi k\rho}} C_1(\varphi, \varphi_0) \tag{72}$$

$$C_1(\varphi, \varphi_0) = D_1(\varphi, \varphi_0) + \sum_q \Gamma_q \frac{1 - F\left(2k\rho \cos^2 \frac{\varphi - \varphi_q - \pi}{2}\right)}{\cos \frac{\varphi - \varphi_q - \pi}{2}} \tag{73}$$

where $\Gamma_q$ are the coefficients of the GO components with outward direction $\varphi_q$ and the function $F(z)$ is the Kouyoumjian-Pathak transition function defined in [22] and its application in the framework of WH formulations is reported in (63) of [25].

The uniform expression of the total far-field is given by

$$E_z(x, y) = E_z^i(\rho, \varphi) + E_z^{utd}(\rho, \varphi) + E_z^{r1}(\rho, \varphi) + E_z^{r2}(\rho, \varphi) \tag{74}$$

From a mathematical point of view, we observe that the UTD is necessary when the SDP crosses the poles related to GO plane wave components (in our problem the reflected waves from the two half-planes).

In particular we will see in the next section that the pole $\eta_o$ generates shadow boundaries for the reflected waves of the two half planes and UTD will be able to compensate effectively the jump of the GO field.

### *5.2. Total far-field in region 3*

In order to compute the total field in region 3 we follow the steps reported for region 1 by noting that in region 3 no primary field is present therefore the Fourier transform of the total field $E_z(x, y)$ in region 3 ($y < -d$) is given by

$$v(\eta, y) = v^m(\eta, y) = v^m(\eta, -d) e^{+j\xi y} \tag{75}$$

where $v^m(\eta, y)$ is the contribution of equivalent magnetic current on the support of the aperture ($x < s, y = -d$) necessary to fulfill the equivalence theorem in region 3 for the original problem, where

$$v(\eta, -d) = v^m(\eta, -d) = V_{2\pi+}(-\eta)e^{j\eta s} \tag{76}$$

In region 3 we note that the GO components are constituted of rays with limited $x$-support at $x < s, y = -d$ therefore their Laplace transforms do not present pole singularities.

With reference to Fig. 1, let us use also the coordinate systems centered on $O'$, i.e. $(x_2, y_2, z)$ and $(\rho_2, \varphi_2, z)$, and the related Fourier transforms. We redefine $v^m(\eta, y) = v(\eta, y) = \tilde{v}(\eta, y_2)e^{j\eta s} = \tilde{v}^m(\eta, y_2)e^{j\eta s}$ related to $\tilde{E}_z(x_2, y_2) = E_z(x, y)$ and therefore $\tilde{v}(\eta, y_2 = 0) = V_{2\pi+}(-\eta)$.

The application of the generalized inverse Fourier transform to $\tilde{v}(\eta, y_2)$ allows to evaluate the total field in any point of region 3:

$$\tilde{E}_z(x_2, y_2) = \tilde{E}_z^m(x_2, y_2) = \frac{1}{2\pi}\int_{\tilde{B}} V_{2\pi+}(-\eta)e^{j\xi(\eta)y}e^{-j\eta\, x_2}d\eta \tag{77}$$

where $\tilde{B}$ is a horizontal line in the convergence region that in this case can be selected as the real axis for the absence of pole singularities. Note that $\tilde{E}_z(x_2, y_2)$ is composed of only the diffracted field.

The use of polar coordinates $(\rho_2, \varphi_2)$ with origin $O' : (x_2, y_2) = (0, 0)$ and the application of the steepest descent path (SDP) method [17] to (77) it yields

$$\tilde{E}_z(\rho_2, \varphi_2) = \tilde{E}_z^m(\rho_2, \varphi_2) = \tilde{E}_z^{SPD}(\rho_2, \varphi_2) \tag{78}$$

where $\tilde{E}_z^{SPD}(\rho_2, \varphi_2)$ is the contribution of the line integral along the SDP approximated as

$$\tilde{E}_z^{SPD}(\rho_2, \varphi_2) = \tilde{E}_z^d(\rho_2, \varphi_2) = E_o\frac{e^{-j(k\rho_2+\pi/4)}}{\sqrt{2\pi k\rho_2}}D_3(\varphi_2, \varphi_o) \tag{79}$$

with

$$D_3(\varphi_2, \varphi_o) = \frac{k\tilde{v}(k\cos\varphi_2, 0)\sin\varphi_2}{jE_o} = \frac{kV_{2\pi+}(-k\cos\varphi_2)\sin\varphi_2}{jE_o} \tag{80}$$

$D_3(\varphi_2, \varphi_o)$ is the GTD diffraction coefficient in region 3 and $\tilde{E}_z^d(\rho_2, \varphi_2)$ is a cylindrical wave with origin $O'$.

Note that in the estimation of (78) we have considered the locations of: the SDP path, the saddle point $\eta_s = k\cos\varphi_2$ where $\varphi_2$ is the observation direction.

In this case the total field is constituted of just the GTD component and since no GO component of infinite support is present, uniformization is not required. In fact, from a mathematical point of view, we observe that the spectrum $\tilde{v}(\eta, y_2)$ in region 3 does not contain any GO pole.

*5.3. Energy flux from region 1 to region 3*

In order to compute the energy flux from region 1 toward region 3 with the assumption of vanishing losses we can proceed in two ways:

1. to compute in physical domain the Poynting vector and integrate it along the aperture $x < s, y = -d$ or by approximation at far field.
2. to compute energy flux via the Parseval theorem, by using directly the spectra along the aperture $x < s, y = -d$.

We observe that the propagation of errors can rise in the computation of energy flux in physical domain. In fact, we need to perform either the computation of near field by inverse Fourier transform or the asymptotic evaluation of the diffracted field at far field before integration of Poynting vector. At near field the integration is performed on the aperture, while at far field on a semi-circumference with center $O'$.

On the contrary, option 2 allows to directly evaluate the energy flux via the integration of the spectra, therefore without any further approximations except the one done for the solution of the WH problem reduced to Fredholm integral equations. However, in the numerical examples of next Section, we show that option 1 at far-field and option 2 give very similar/almost coincident results.

Let us now show how to obtain the energy flux with the two options. The energy flux $P_3$ toward region 3 is given by the integration of the real part of the Poynting vector $\tilde{\mathbf{S}} = \frac{1}{2}\tilde{\mathbf{E}} \times \tilde{\mathbf{H}}^*$ along the aperture $x_2 < 0, y_2 = 0$ with normal

$-\hat{y}_2$:

$$P_3 = \int_{-\infty}^{0} Re[\tilde{S}_y(x_2, y_2 = 0)]dx_2 \tag{81}$$

where $\tilde{S}_y$ is the $y$ component of the Poynting vector

$$\tilde{S}_y(x_2, y_2) = \frac{1}{2}\tilde{E}_z(x_2, y_2)\tilde{H}_x^*(x_2, y_2) \tag{82}$$

With the assumption of vanishing losses, by using polar coordinates, and considering that at far field $\tilde{E}_z(\rho_2, \varphi_2)$ is given by (78)-(80) and $\tilde{H}_{\varphi_2}(\rho_2, \varphi_2) = \frac{1}{Z_o}\tilde{E}_z(\rho_2, \varphi_2)$, we obtain.

$$P_3 = \int_{-\pi}^{0} Re[\tilde{S}_y(\rho_2, \varphi_2)]\rho_2 d\varphi_2 = \int_{-\pi}^{0} Re[\frac{1}{4\pi k Z_o}]|D_3(\varphi_2, \varphi_o)|^2 d\varphi_2 \tag{83}$$

with $D_3(\varphi_2, \varphi_o)$ reported in (80). Alternatively $P_3$ can be computed via the spectra. In particular we write (81) with the help of Parseval theorem

$$\begin{aligned} P_3 &= \int_{-\infty}^{0} \tfrac{1}{2} Re[\tilde{E}_z(x_2, y_2 = 0)\tilde{H}_x^*(x_2, y_2 = 0)]dx_2 = \\ &= \tfrac{1}{2\pi} \int_{-\infty}^{+\infty} \tfrac{1}{2} Re[\tilde{v}(\eta, y_2 = 0)\tilde{i}^*(\eta, y_2 = 0)]d\eta \end{aligned} \tag{84}$$

We recall that (46) is valid also for *tilde* functions and by considering that $\tilde{v}(\eta, y_2 = 0) = V_{2\pi+}(-\eta)$ we obtain

$$P_3 = \frac{1}{2\pi} \int_{-\infty}^{+\infty} \frac{1}{2}|V_{2\pi+}(-\eta)|^2 Re[Y_\infty^*(\eta)]d\eta \tag{85}$$

## 6. Validation and Numerical Examples

With reference to the problem reported in Fig. 1, in this Section we provide validations and numerical examples of the proposed method in relation to the geometrical and physical parameters: $s$, $d$ and $\varphi_o$ with $E_o = 1V/m$. We recall that while $s < 0$ the two half-planes generate a section of parallel PEC plane waveguide of length $|s|$.

As stated in Section 1, to meet mathematical requirements of the WH technique small vanishing losses are assumed in the medium, i.e. $k = k' - jk''$ where $k', k'' > 0$ and $k''/k' << 1$ (negligible losses, i.e. $k''/k' = 10^{-8}$).

For computational purpose we have selected $k' = 1$. The analysis of problem for practical values of geometrical/electromagnetic parameters is obtainable by scaling the quantities according to [28]. In particular a different value of $k'$ (for example $k' = p$ that it yields for example $k_{new} = p(1 - j10^{-8})$) changes the computed spectrum $F_+(\eta)$ to $\frac{k}{k_{new}} F_+(\frac{k\eta}{k_{new}})$, and the distance $d$ and $s$ becomes respectively $kd/k_{new}$ and $ks/k_{new}$ (since in our formulation the dependence on $d$ and $s$ appears always as $kd$ and $ks$ thus all the quantities are invariant for constant $kd$ and $ks$).

In the following we make self-convergence tests and validation thorough an independent full numerical solution obtained by a in-house code based on the Finite Element Method (FEM) [33] with the following setup: region truncated at a distance of $\rho = 20 \div 30\,\lambda$ from the origin $O$ with perfectly matched layer of cylindrical shape of depth $\lambda/2$ and discretization via triangles with max side length of $\lambda/8$. Although we have truncated the structure at a huge distance from the origin, the truncation generates spurious diffraction/reflections of the incident plane wave that compromise the precision of the FEM solution in region 3 in particular for overlapped half planes ($s < 0$). On the contrary our semi-analytical method does not suffer of such limit and this phenomenon demonstrates its superiority for the analysis of infinite canonical problems. In the following, we also illustrate the properties of the solution for practical cases and we present physical and engineering insights for applications in the field of antenna technologies, electromagnetic compatibility and electromagnetic shielding by estimating the following parameters/quantities: GTD/UTD diffraction coefficients, total far fields, transmitted scattered energy flux.

### *6.1. Test case 1: experimental test on convergence*

In order to focus the attention on the validation of our technique we illustrate in depth in this subsection the convergence properties for the problem under

examination with the following physical parameters: $E_o = 1V/m$, $k = k' - jk'' = 1 - j10^{-8}m^{-1}$, $\varphi_o = 0.25\pi$, $k's = 1$, $k'd = 1$. In particular to stress our numerical solution we select a contour warping in (60) with a relaxed parameter $\theta = \theta_c = \pi/4$ (61), as discussed at the end of previous section. We have also checked to obtain almost coincident results by applying $0 \ll \theta \lesssim \theta_c$ for instance $\theta = 0.23\pi$. To check convergence we modify the integration parameters $A$ and $h$. In Fig.6 we illustrate the convergence on the absolute value of the spectral components for a fixed $A = 60$ and a variable $h \in [0.1, 5]$. For each spectral component and selection of integration parameters we have estimated the relative error in $log_{10}$ scale with respect to the reference solution $A = 100$, $h = 0.05$. The plotted numerical results demonstrate the convergence for $h \geq 0.2$. In Fig.7 we illustrate the convergence on the absolute value of the spectral components for a fixed $h = 0.1$ and a variable $A \in [5, 60]$. For each spectral component and selection of integration parameters we have estimated the relative error in $log_{10}$ scale with respect to the reference solution $A = 100$, $h = 0.05$. The Figure demonstrates the convergence for $A \geq 50$. Relative errors less of approx $10^{-3}$ have very low impact on the estimation of field components in the physical domain as it will be demonstrated in next test cases.

### *6.2. Test case 2: variable $k's$, fixed $k'd = 1$*

In this test case we illustrate the solution of the problem under examination (Fig. 1) in terms of physical engineering quantities/parameters for a fixed $k'd = 1$, variable $k's$ and different incidence angles $\varphi_o$. In particular we show plots of the total far-field in region 1 (74) and region 3 (78); we also show the energy flux toward region 3 (83),(85).

Fig.8 shows on the left the total far field in region 1 at $k'\rho = 10$ with respect to the origin $O$ (Fig. 1) and its composition in terms of GO and UTD components for $k's = -3, 3$, $k'd = 1$, $\varphi_o = 0.25\pi$,$E_o = 1V/m$ with $k = 1 - j10^{-8}m^{-1}$ obtained via discretization of (60) with an integration contour parameter $\theta \lesssim \theta_c$ (61) and integration parameters $A = 60, h = 0.1$ useful to obtain good convergence (see test case 1). In the same figure on the right side we have reported the

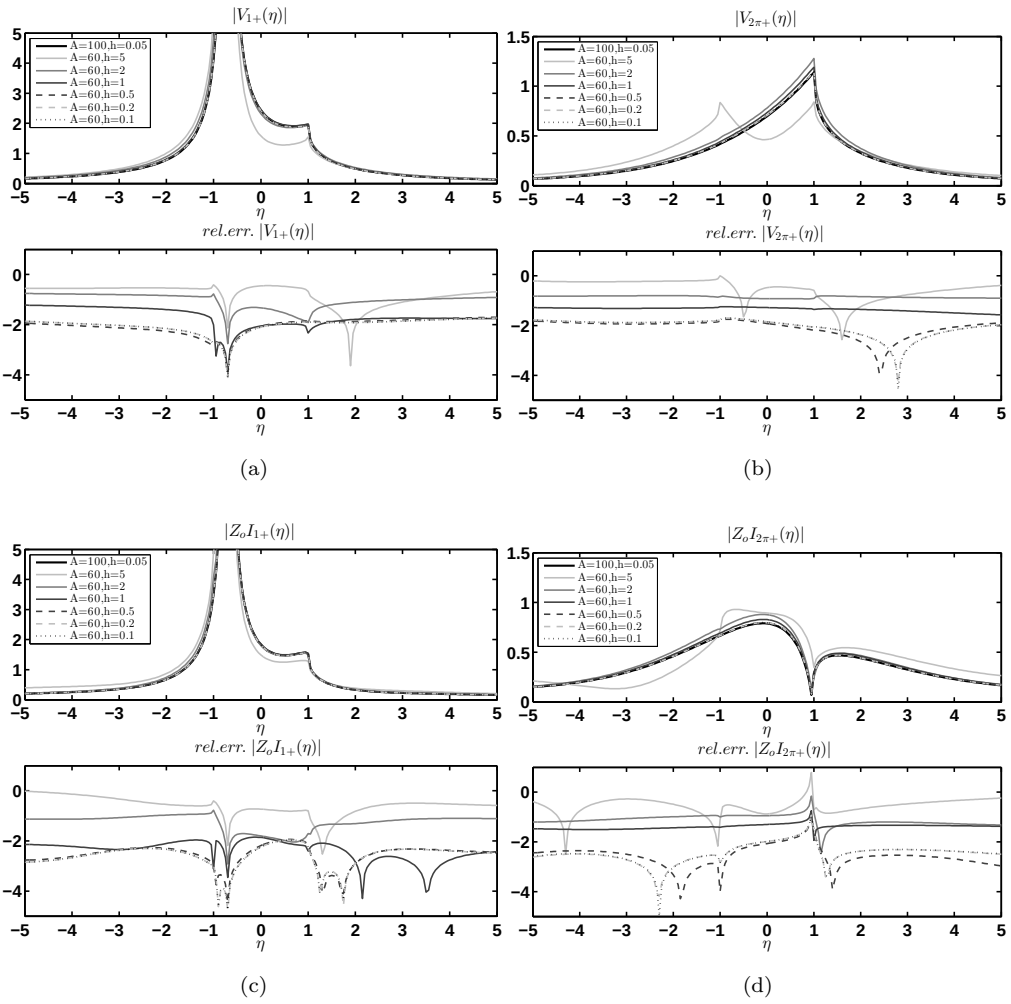


Figure 6: Test Case 1. Convergence of spectral components for $A = 60$ and $h \in [0.1, 5]$: plots of absolute value and the relative error in $log_{10}$ scale with respect to the reference solution $A = 100, h = 0.05$ for real values of $\eta$. (a) $V_{1+}(\eta)$, (b) $V_{2\pi+}(\eta)$, (c) $Z_oI_{1+}(\eta)$, (d) $Z_oI_{2\pi+}(\eta)$.

comparison between the solution proposed in this paper and the FEM solution (see description at the beginning of this section for details) in terms of total far-field at $k'\rho = 10$.

We note that in the case $k's = -3$ we obtain a section of parallel PEC plate waveguide of length $|k's| = 3$ and distance between planes that is $k'd = 1$.

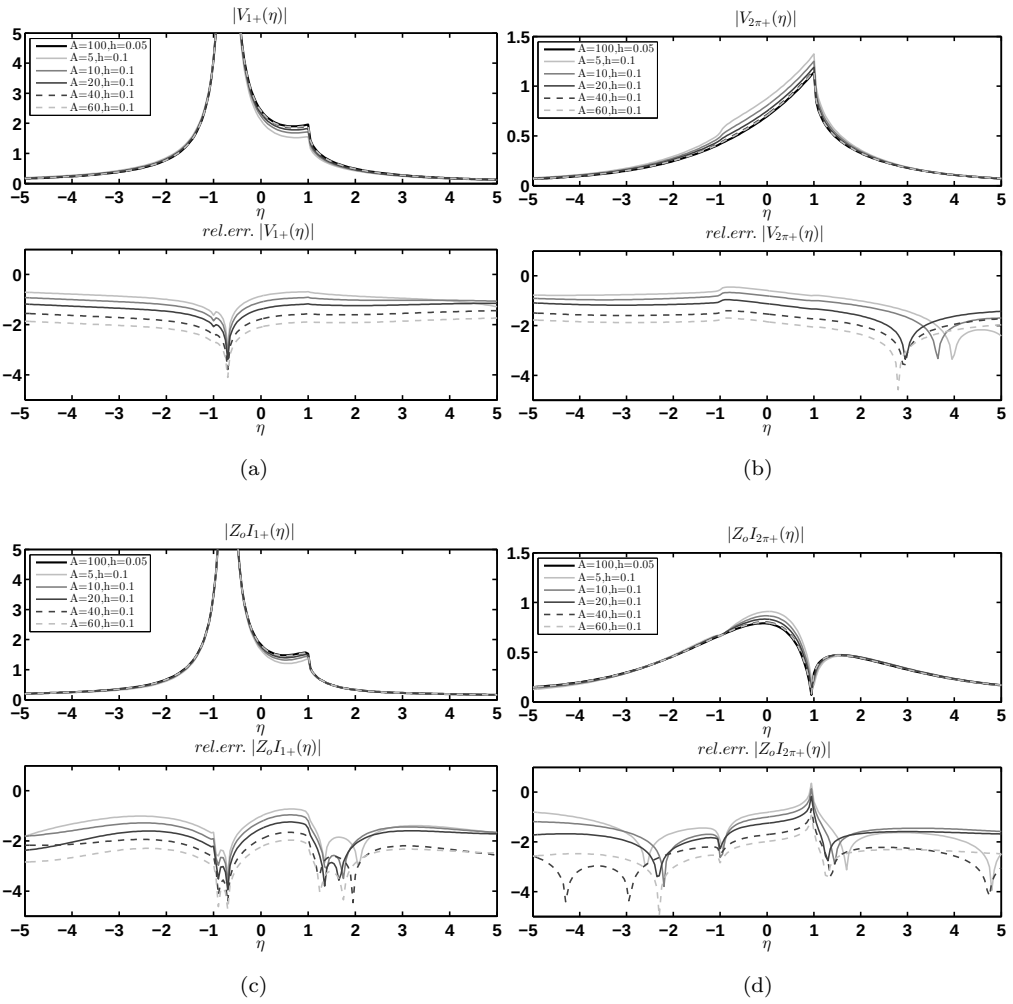


Figure 7: Test Case 1. Convergence of spectral components for $h = 0.1$ and $A \in [5, 60]$: plots of absolute value and the relative error in $log_{10}$ scale with respect to the reference solution $A = 100, h = 0.05$ for real values of $\eta$. (a) $V_{1+}(\eta)$, (b) $V_{2\pi+}(\eta)$, (c) $Z_oI_{1+}(\eta)$, (d) $Z_oI_{2\pi+}(\eta)$.

In this case the parallel PEC plate waveguide is in cutoff (no propagating $TE_z$ mode along $x$) since the x-propagation constant $k_{xn} = \sqrt{k^2 - k_{tn}^2}$ is with strong imaginary part as $k_{tn} = n\pi/d$ for any $n \in \mathbb{N}_0$. The cutoff condition for the $TE_z$ $n$ mode can be expressed as $k' < k_{tn} = n\pi/d$, i.e. non-propagating $TE_z$ $n$ modes are with $k'd < n\pi$.

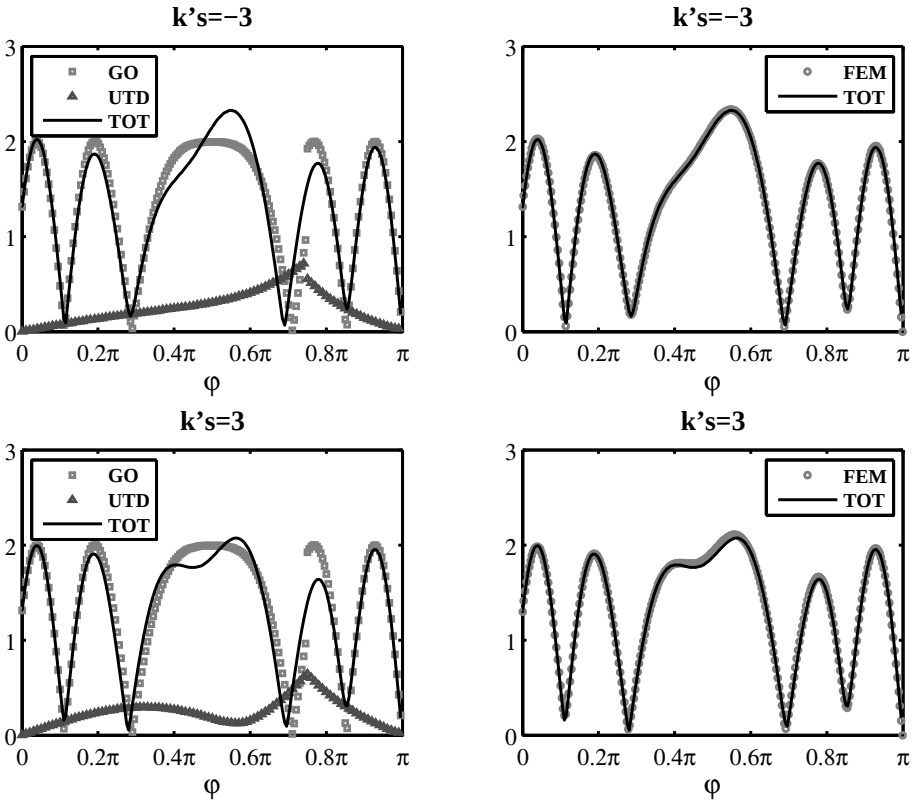


Figure 8: Test case 2. Left: total far field [V/m] in region 1 at $k'\rho = 10$ and its composition in terms of GO and UTD components for $k's = -3(3)$ on top (bottom) and $k'd = 1$, $\varphi_o = 0.25\pi$,$E_o = 1V/m$ with $k = 1 - j10^{-8}m^{-1}$ obtained via discretization of (60) with $\theta \lesssim \theta_c$, $A = 60$, $h = 0.1$. Right: comparison of total far field [V/m] with FEM solution as described in the main text.

Fig.9 shows on the left the total far field in region 3 at $k'\rho_2 = 10$ with respect to the origin $O'$ (Fig. 1) for the case $k's = -3$, while on the right the same result for $k's = 3$ (see Sections 5.2, 5.3 and the Introduction for the quantities defined with coordinates $(x_2, y_2, z)$ or $(\rho_2, \varphi_2, z)$ centered at $O'$).Both sub-figures also report the FEM solution. In particular on the left for $k's = -3$, we are in presence of a section of parallel PEC plate waveguide at cutoff, therefore the field of region 3 is very weak. As anticipated at the beginning of the section, the FEM solution is not able to model the field because the spurious field generated

by the truncation of the geometry is stronger than the physical one. Moreover, on the right side of the same figure we see similar strength of field in region 3 but loss in precision on FEM case due to the spurious field that slightly changes the direction of maximum and generates oscillations.

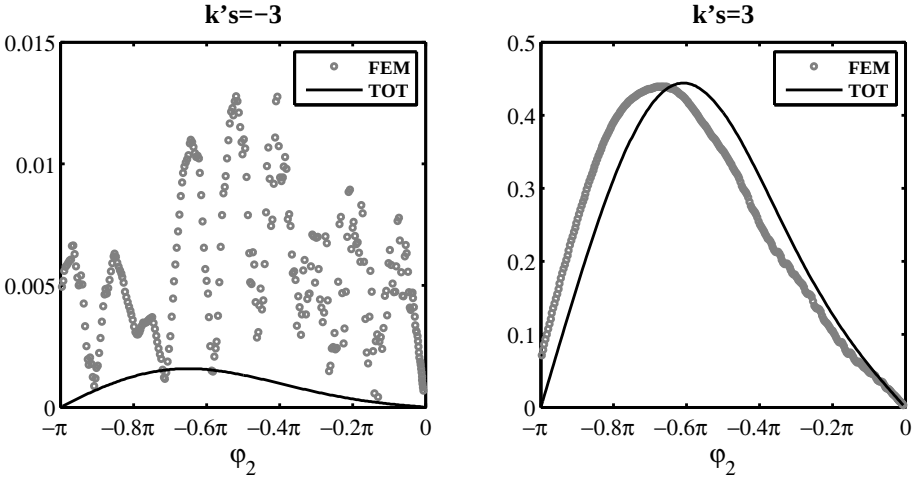


Figure 9: Test case 2. Left: total far field [V/m] in region 3 at $k'\rho_2 = 10$ for $k's = -3$ with the proposed method and FEM solution. Right: total far field [V/m] at $k'\rho_2 = 10$ for $k's = 3$ with the proposed method and FEM solution. $k'd = 1$, $\varphi_o = 0.25\pi$,$E_o = 1V/m$ with $k = 1 - j10^{-8}m^{-1}$

Fig.10 presents the total far field in region 1 and 3 with same geometrical and physical parameters except for the incident angle $\varphi_o = 0.75\pi$ instead of $\varphi_o = 0.25\pi$ that yields different regularity properties of the spectral functions due to the location of the pole $\eta_o$. Fig. 11 shows on the left side the energy flux toward region 3 (85) in $dB$ ($10\log_{10} P_3$) for different values of overlap parameter $k's$ maintaining $k'd = 1$, $\varphi_o = 0.25\pi$,$E_o = 1V/m$ with $k = 1 - j10^{-8}m^{-1}$. On the right side the figure shows the relative error with respect to (83) in $\log_{10}$ scale.

### *6.3. Test case 3: variable $k's$, fixed $k'd = 5$*

As discussed in test case 2, while $s < 0$ the two half-planes overlap and create a section of parallel PEC plate waveguide whose $TE_z$ modes propagate along

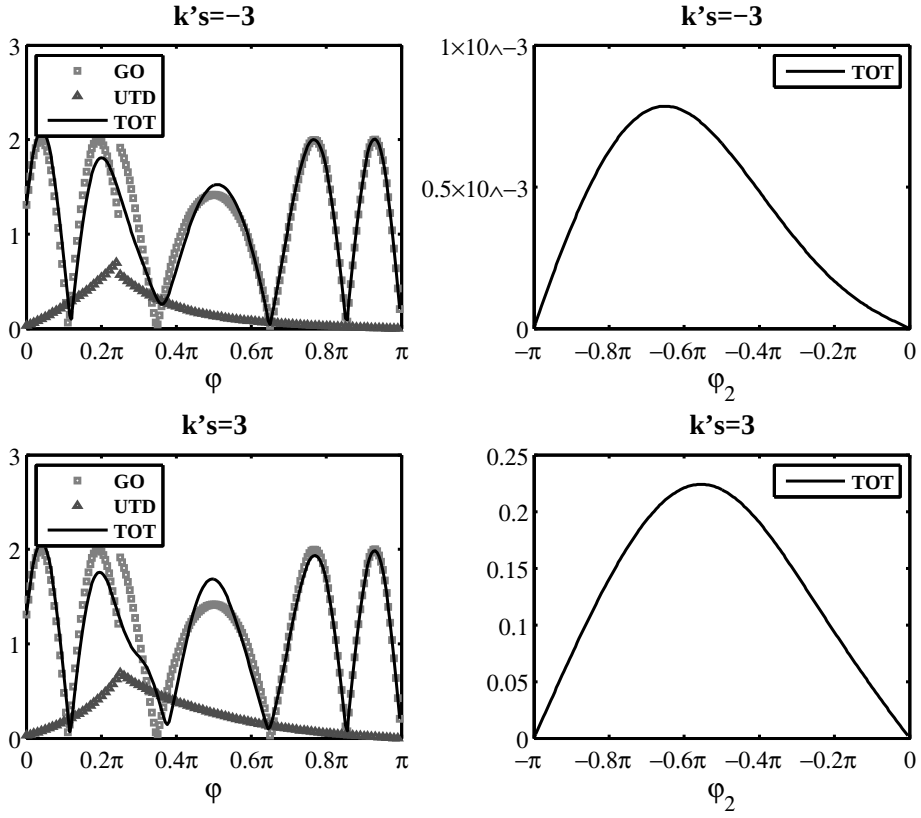


Figure 10: Test case 2. Left: total far field [V/m] in region 1 at $k'\rho = 10$ and its composition in terms of GO and UTD components for $k's = -3(3)$ on top (bottom) and $k'd = 1$, $\varphi_o = 0.75\pi$,$E_o = 1V/m$ with $k = 1 - j10^{-8}m^{-1}$ obtained via discretization of (60) with $\theta \lesssim \theta_c$, $A = 60$, $h = 0.1$. Right: total far field [V/m] in region 3 at $k'\rho_2 = 10$ for $k's = -3(3)$ on top (bottom) and $k'd = 1$, $\varphi_o = 0.75\pi$,$E_o = 1V/m$ with $k = 1 - j10^{-8}m^{-1}$.

$-x$ with x-propagation constant $k_{xn} = \sqrt{k^2 - k_{tn}^2}$ ‘ ($k' < k_{tn} = n\pi/d$, $n \in \mathbb{N}_0$). With the assumptions $\varphi_o = 0.25\pi$,$E_o = 1V/m$ with $k = 1 - j10^{-8}m^{-1}$, the cutoff condition for the $TE_z$ $n$ mode can be expressed as $k' < k_{tn} = n\pi/d$, i.e. non-propagating $TE_z$ $n$ modes are with $k'd < n\pi$. The propagation of modes over cut-off yields a stronger energy flux toward region 3 (in comparison to test case 2).

In this test case we have selected $k'd = 5$ and the numerical results are

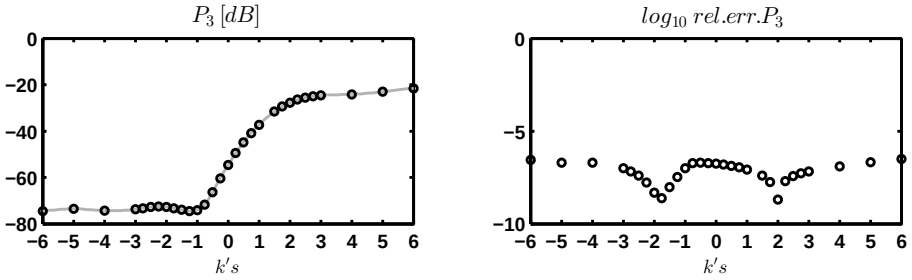


Figure 11: Test case 2. Left: energy flux toward region 3 (85) in $dB$ ($10\log_{10} P_3$) for different values of overlap parameter $-6 \leq k's \leq 6$ maintaining $k'd = 1$, $\varphi_o = 0.25\pi$,$E_o = 1V/m$ with $k = 1 - j10^{-8}m^{-1}$. Right: relative error of (85) with respect to (83) in $\log_{10}$ scale.

obtained via discretization of (60) with $\theta \lesssim \theta_c$, $A = 60$, $h = 0.1$. Since $\pi < k'd < 2\pi$, only the first (fundamental) $TE_z$ is above cutoff and it propagates along $-x$ where the propagation constant $k_{x1}$ have a strong real part and vanishing imaginary part due to $k''$:

$$k_{x1} = \sqrt{k^2 - k_{t1}^2} \backsimeq 0.778k' \tag{86}$$

Fig. 12 shows on the left the total far field in region 1 at $k'\rho = 10$ with respect to the origin $O$ (Fig. 1) for the test case with $k's = -8, -3, 3, 8$; while on the right the total far field in region 3 at $k'\rho_2 = 10$ with respect to the origin $O'$ (Fig. 1) for the corresponding $k's$. We note that in this case the overlap and non-overlap cases yield similar energy fluxes because of the fundamental $TE_{z1}$ mode propagation. For the case $k's = -3$, we have propagation of the $TE_z$ $n = 1$ mode with axial oscillations in a number of $k_{x_1}|s|/(2\pi) = 3{*}0.778/(2/pi) = 0.37cycles$ while for $k's = -8$ we have $k_{x_1}|s|/(2\pi) = 8 * 0.778/(2/pi) = 0.99cycles$. For $k's = 3, 8$ we observe energy fluxes due to the aperture with radiation shape depending on its size (see right side of Fig. 12). Fig. 13 shows on the left side the energy flux toward region 3 (85) in linear scale for different values of overlap parameter $k's$ maintaining $k'd = 5$, $\varphi_o = 0.25\pi$,$E_o = 1V/m$ with $k = 1 - j10^{-8}m^{-1}$. On the right side the figure shows the relative error with respect to (83) in $\log_{10}$ scale. With respect to test case 2, we observe that while $s < 0$ the energy flux toward region 3 is substantial and independent from $|s|$

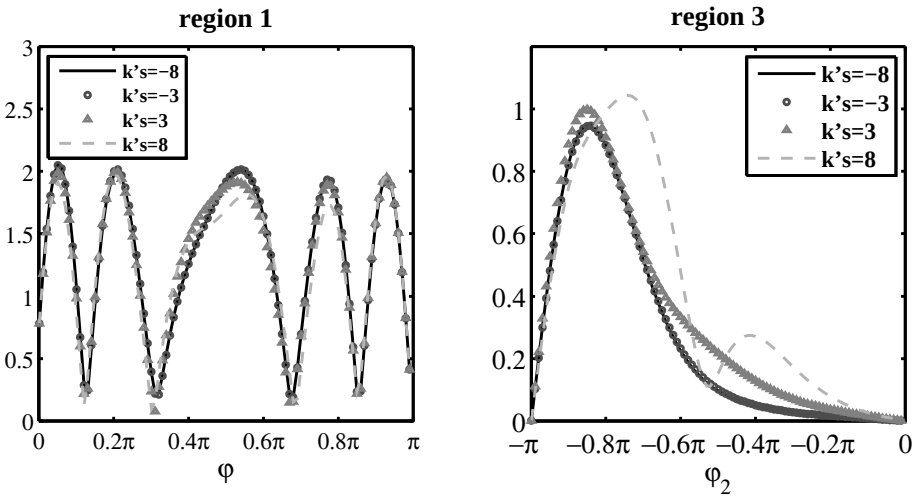


Figure 12: Test case 3. Left: total far field [V/m] in region 1 at $k'\rho = 10$ for $k's = -8, -3, 3, 8$, $\varphi_o = 0.25\pi$,$E_o = 1V/m$ with $k = 1 - j10^{-8}m^{-1}$. Right: total far field [V/m] in region 3 at $k'\rho_2 = 10$ for the corresponding cases.

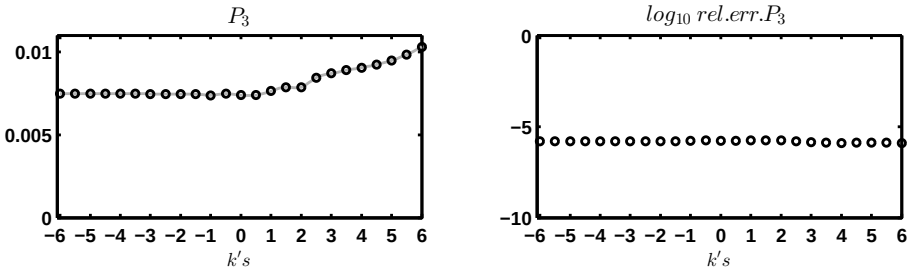


Figure 13: Test case 3. Left: energy flux toward region 3 (85) in linear scale ($P_3$) for different values of overlap parameter $-6 \leq k's \leq 6$ maintaining $k'd = 5$, $\varphi_o = 0.25\pi$,$E_o = 1V/m$ with $k = 1 - j10^{-8}m^{-1}$. Right: relative error of (85) with respect to (83) in $\log_{10}$ scale.

due to the guiding properties of the parallel PEC plate waveguide.

### *6.4. Test case 4: almost coplanar case $k'd \to 0$, $k's > 0$*

In this test case we illustrate a further validation of our method. We stress the proposed procedure with the limit $k'd \to 0$. When $k'd \to 0$, the two half-planes are almost coplanar and therefore the fields $E_z(x, y = 0)$ and the field $E_z(x, y = -d)$ are expected to exhibit similar behaviour in particular

along the aperture $0 < x < s$. To demonstrate this we evaluate and compare the spectrum of $V_{1+}(\eta)$ and $V_{2\pi+}(-\eta)e^{j\eta s}$ that are respectively the x-Laplace transform of the electric fields at $y = 0$ and $y = -d$, according to Section 2. Fig. 14 reports the comparison between the spectrum of $V_{1+}(\eta)$ and $V_{2\pi+}(-\eta)e^{j\eta s}$ in terms of absolute value, argument and relative error of $V_{1+}(\eta)$ with respect to $V_{2\pi+}(-\eta)e^{j\eta s}$ for the following physical and geometrical parameters: $k'd = 10^{-3}$, $k's = 1$, $\varphi_o = 0.25\pi$,$E_o = 1V/m$ with $k = 1 - j10^{-8}m^{-1}$. Fig. 15 shows

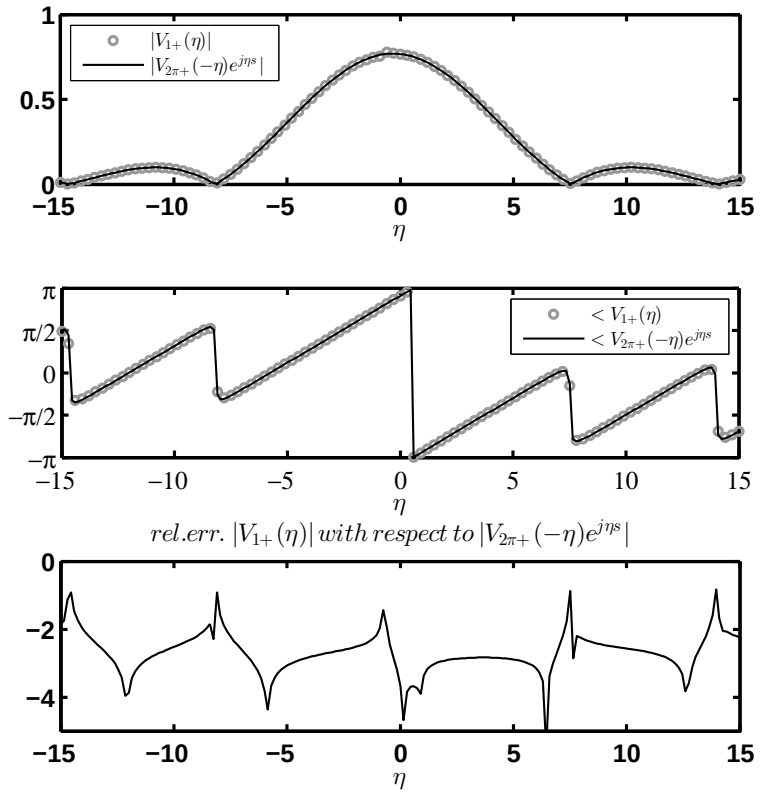


Figure 14: Test case 4. Top: absolute values of $V_{1+}(\eta)$ and $V_{2\pi+}(-\eta)e^{j\eta s}$. Center: Argument of $V_{1+}(\eta)$ and $V_{2\pi+}(-\eta)e^{j\eta s}$. Bottom: $V_{1+}(\eta)$ with respect to $V_{2\pi+}(-\eta)e^{j\eta s}$ in $\log_{10}$ scale.

the far field in region 1 and 3 for the test case. In region 1 the UTD component is necessary to estimate the diffraction phenomenon but with respect to the previous test cases the GO component does not exhibit jumps since the reflected

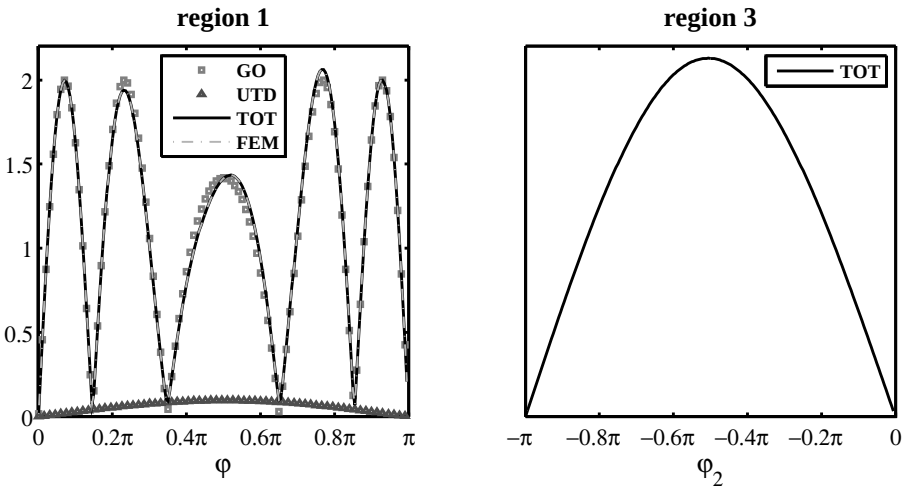


Figure 15: Test case 4. Left: total far field [V/m] in region 1 at $k'\rho = 10$ and its composition in terms of GO and UTD components for $k'd = 10^-3$, $k's = 1$ $\varphi_o = 0.25\pi$,$E_o = 1V/m$ with $k = 1 - j10^{-8}m^{-1}$ obtained via discretization of (60) with $\theta \lesssim \theta_c$, $A = 60$, $h = 0.1$; the same subfigure reports the total far filed obtained via FEM solution as described on top of the section. Right: total far field [V/m] in region 3 at $k'\rho_2 = 10$ obtained with the proposed method.

.

waves of the two half planes are almost completely in phase and coplanar. The solution is obtained via discretization of (60) with $A = 60$, $h = 0.1$ and $\theta \lesssim \theta_c$, i.e. $\theta_c \backsimeq d/s = 10^-3$. Although we are forced to select an integration contour near the real axis of $\eta$ plane, the spectral properties of the kernels improves by yielding high precision results as demonstrated by comparison with the FEM solution (see region 1 in Fig. 15 the TOT and FEM curves are coincident).

## 7. Conclusion

In this work we have described the scattering of a plane electromagnetic wave by two opposite staggered perfectly electrically conducting (PEC) half-planes immersed in free space by using the Wiener-Hopf technique in the spectral domain. We have proposed a novel effective semi-analytical method for the solution, that is based on the reduction of the factorization problem of matrix

Wiener-Hopf equations to Fredholm integral equations of second kind. Several numerical test cases validate the proposed method. The structure is of interest in antenna technologies, electromagnetic compatibility and electromagnetic shielding in particular for what concerns the computation of the transmitted field. From a mathematical point of view the paper presents a novel effective technique to handle WH formulations with exponential behavior.

**Acknowledgments**

All the data used are reported in the paper, references, tables, and figures. This work is partially supported by Politecnico di Torino, Torino Italy and the Istituto Superiore Mario Boella (ISMB), Torino, Italy.

**References**

[1] I.D. Abrahams, "Scattering of sound by two parallel semi-infinite screens," *Wave Motion,* 9, 289-300 (1987)

[2] I.D. Abrahams, G.R. Wickham, "On the scattering of sound by two semi-infinite parallel staggered plates. I. Explicit matrix Wiener-Hopf factorization," *Proc. Royal Soc. London*, A420, 131155 (1988)

[3] I.D. Abrahams, G.R. Wickham, "The scattering of water waves by two semi-infinite opposed vertical walls," *Wave Motion,* 14, 145-168 (1991)

[4] A. Kisil, L. Ayton, "Aerodynamic noise from rigid trailing edges with finite porous extensions," *Journal of Fluid Mechanics,* 836, 117-144 (2018).

[5] D.S Jones, "Diffraction by three semi-infinite planes," *Proc. R. Soc. Lond.,* A404, 299-321 (1986)

[6] B. Noble, "Methods Based on the Wiener-Hopf Technique for the Solution of Partial Differential Equations," Pergamon Press, London,(1958)

[7] M. Idemen, "A new method to obtain exact solutions of vector WienerHopf equations," *Zeit Angew Math Mech,* 59, 656658 (1979)

[8] A.D. Rawlins, "Simultaneous Wiener-Hopf equations," *Canad. J. Phys.,* 58, 420-429 (1980)

[9] A. Büyükaksoy, H. Serbest, "Matrix Wiener-Hopf Factorization Methods and Applications to Some Diffraction Problems," Chapter 6, pp. 257-315, of M. Hashimoto, M. Idemen and O.A. Tretyakov, *Analytical and Numerical Methods in Electromagnetic Wave Theory*, Tokyo, Japan: Science House Co. Ltd. (1993)

[10] A. Büyükaksoy, E. Topsakal, M. Idemen, "Plane wave diffraction by a pair of parallel soft and hard overlapped half-planes," *Wave Motion,* 20, 273-282 ( 1994)

[11] J.-P. Zheng, K. Kobayashi, "Diffraction by a semi-infinite parallel-plate waveguide with sinusoidal wall corrugation: combined perturbation and wiener-hopf analysis," *Progress In Electromagnetics Research B,* 13, 75-110 (2009)

[12] S.C. Kashyap, "Diffraction characteristics of a slit formed by two staggered parallel planes," *J. Math. Phys.,* 15, 1944-1949 (1974).

[13] I.D. Abrahams and G.R. Wickham, "General WienerHopf Factorization of Matrix Kernels with Exponential Phase Factors," *SIAM J. Appl. Math.,* 50, 819-838 (1990).

[14] I.D. Abrahams, G.R. Wickham, "Acoustic scattering by two parallel slightly staggered rigid plates," *Wave Motion,* 12, 281-297 (1990).

[15] V.G. Daniele, G. Lombardi, "Fredholm factorization of Wiener-Hopf scalar and matrix kernels," *Radio Sci.,* 42: RS6S01, 1-19 (2007).

[16] V.G. Daniele, R.S. Zich, *The Wiener Hopf method in Electromagnetics,* Scitech Publishing (2014)

[17] L.B. Felsen, N. Marcuvitz, *Radiation and Scattering of Waves,* Englewood Cliffs, NJ: Prentice-Hall (1973)

[18] V.G. Daniele, R.D. Graglia, G. Lombardi, P.L.E. Uslenghi, "Cylindrical resonator sectorally filled with DNG metamaterial and excited by a line source," *IEEE Antennas Wireless Propag. Lett.,* 11:6286981, 1060-1063 (2012).

[19] V.G. Daniele, G. Lombardi, R.S. Zich, "Network representations of angular regions for electromagnetic scattering," *Plos One,* 12(8):e0182763, 1-53 (2017)

[20] V.G. Daniele, G. Lombardi, R.S. Zich, "The electromagnetic field for a PEC wedge over a grounded dielectric slab: 1. Formulation and validation," *Radio Science,* 52, 1-20 (2017)

[21] V.G. Daniele, G. Lombardi, R.S. Zich, "The electromagnetic field for a PEC wedge over a grounded dielectric slab: 2. Diffraction, Modal Field, SurfaceWaves, and Leaky Waves," *Radio Science,* 52, 1-18 (2017)

[22] R.G. Kouyoumjian, P.H. Pathak, "A uniform geometrical theory of diffraction for an edge in a perfectly conducting surface," *Proc. IEEE.,* 62, 1448-1461 (1974)

[23] J. Meixner, "The behavior of electromagnetic fields at edges," *IEEE Trans. Antennas Propag.,* 20, 442-446 (1972).

[24] L.V. Kantorovich, V.I. Krylov, *Approximate methods of higher analysis,* Groningen, The Netherlands: Noordhoff (1964).

[25] V.G. Daniele and G. Lombardi, "Wiener-Hopf Solution for Impenetrable Wedges at Skew Incidence," *IEEE Trans. Antennas Propag.,* 54, 2472-2485 (2006).

[26] V.G. Daniele and G. Lombardi,"The Wiener-Hopf Solution of the Isotropic Penetrable Wedge Problem: Diffraction and Total Field," *IEEE Trans. Antennas Propag.,* 59, 3797-3818 (2011).

[27] V.G. Daniele, G. Lombardi, "Arbitrarily oriented perfectly conducting wedge over a dielectric half-space: diffraction and total far field," *IEEE Trans. Antennas Propag.,* 64:4, 1416-1433 (2016).

[28] V.G. Daniele, "Electromagnetic Fields for Perfectly Electrical Conducting Wedge over Stratified Media: Part I," *Electromagnetics.*, 33:3, 179-200 (2013).

[29] M. Albani, "A uniform double diffraction coefficient for a pair of wedges in arbitrary configuration," *IEEE Trans. Antennas Propag.,* 53:2, 702-710 (2005).

[30] A. Toccafondi, R. Tiberio, "An incremental theory of double edge diffraction," *Radio Science,* 42:RS6S30, 1-13 (2007).

[31] T. Negishi, V. Picco, D. Spitzer, D. Erricolo, G. Carluccio, F. Puggelli, M. Albani, "Measurements to Validate the UTD Triple Diffraction Coefficient," *IEEE Trans. Antennas Propag.,* 62:7, 3723-3730 (2014).

[32] A.V. Osipov, S.A. Tretyakov, *Modern Electromagnetic Scattering Theory with Applications,* Chichester, UK: Wiley (2017).

[33] R.D. Graglia, G. Lombardi, "Singular higher order complete vector bases for finite methods," *IEEE Trans. Antennas Propag.,* 52:7, 1672-1685 (2004).